

# The use of meteorological and oceanographic sensor data in the German offshore territory for the corrosion monitoring of marine structures

A.W. Momber<sup>a,\*</sup>, M. Wilms<sup>b</sup>, D. Brün<sup>c</sup>

<sup>a</sup> Muehlhan AG, Hamburg, Germany

<sup>b</sup> Federal Maritime and Hydrographic Agency (BSH), Hamburg, Germany

<sup>c</sup> Salitation GmbH, Bielefeld, Germany

## ARTICLE INFO

### Keywords:

Cathodic protection  
Data management  
Predictive maintenance  
Sensors  
Signal processing

## ABSTRACT

The use of sensor data is a pre-requirement for the use of Digital Twins and for the integration of data-based maintenance strategies for corrosion protection systems of marine structures. The paper defines the requirements for sensor signals/data for the modeling of corrosion processes in marine environments. Data demands are reviewed, and respective sensor necessity matrices are derived. Meteorological data (for atmospheric corrosion) and oceanographic data (for immersed seawater corrosion), delivered by three environmental sensor networks in the German offshore territory (North Sea, Baltic Sea), are benchmarked and categorized for the first time. Examples for relevant environmental sensor data for the atmospheric as well as for immersed seawater corrosion are presented. Local (micro-environment) and incremental (temporal variations) corrosive loads are characterized based on sensor data. The treatment and 2-step management of sensor data are discussed. An approach for their integration into a data-based monitoring and maintenance model is introduced. Examples are provided for the utilization of sensor data for the monitoring of corrosion processes and for the design of cathodic protection systems.

## 1. Introduction

The use of large amounts of digital data is a general trend in the industry, particularly for monitoring and maintenance purposes. Momber et al. (2021a, 2022) proposed a concept of a fully data-based procedure for the condition monitoring of surface protection systems on steel structures. This concept includes the utilization of environmental (meteorological) sensor data for the evaluation of corrosion processes. Additionally, Digital Twins have found applications in maintenance strategies, where they are used for the prediction of the state of assets, to improve condition monitoring and fault diagnostic, to reduce the number of maintenance activities, and to formulate optimal maintenance intervals (Errandonea et al., 2020; Momber et al., 2021b). From the practical application point of view, virtual models, or twins, combine mathematical models describing the physics of assets' operations with *sensor data* acquired and processed from real assets (physical twin) during their operation under real world conditions. The integration of sensor data is a key feature of any Digital Twin, whereby the real-time sensor data are used for dynamically re-calibrating deterioration and maintenance models for more reliable and precise

decision-making processes (Momber et al., 2021b). The availability, acquisition and processing of signals (sensor data) is an indispensable requirement for any maintenance method applied to structures (e.g. Tchakoua et al., 2014). However, sensor data are particularly important for the introduction of preventive/predictive maintenance processes. A benchmark study performed as part of this study revealed the following challenges associated with the utilization of raw sensor signals:

- missing, inconsistent or defective data;
- time drift;
- different/diverse measurement intervals;
- different/diverse signal formats;
- data import and management are extremely time consuming, especially for historical data;
- data import, treatment and analysis need to be automated;
- large amounts of data (several Gigabyte per year).

The scope and the organization of this contribution are highlighted in Fig. 1 for an offshore wind power turbine. The numbers 3 to 6 refer to the respective chapters in the paper. The contribution is concerned with

\* Corresponding author.

E-mail address: [andreas.momber@t-online.de](mailto:andreas.momber@t-online.de) (A.W. Momber).

the availability, acquisition and processing of signals/data from meteorological and oceanographic sensors in the German offshore territory (North Sea and Baltic Sea) and their integration into an online monitoring and maintenance model for protective systems for marine structures. The novelties of this contribution include the definition of necessary sensor data, a sensor availability study, a two-step sensor signal treatment procedure, and the integration of the sensor data into a data-based condition monitoring model.

## 2. Sensor necessity matrices for corrosion modeling

### 2.1. General form for corrosion models

Meteorological and oceanographic sensors become useful when their data can be integrated into corrosion models. With respect to the corrosion of steels in marine environments, a number of models have been issued over the years. The temporal progress of corrosion can be generalized as follows (Momber, 2022):

$$C_{\text{corr}} = f(t_E, X_i, Y_i) \quad (1)$$

Here,  $C_{\text{corr}}$  is the corrosion attribute,  $t_E$  is the exposure time,  $X_i$  are material parameters (composition, texture, alloying, electrochemical parameters), and  $Y_i$  are external parameters (environmental parameters). Corrosion attributes include corrosion loss/depth (e.g. in  $\mu\text{m}$ ), weight loss (e.g. in g), specific weight loss (e.g. in  $\text{g}/\text{m}^2$ ), corrosion rate (e.g. in  $\mu\text{m}/\text{y}$ ), and pit depth (e.g. in  $\mu\text{m}$ ). This presentation is concerned with the parameters  $Y_i$ , which are either deterministic parameters (fixed values) or random (distributed) parameters. A further categorisation can be performed into primary environmental parameters and secondary environmental parameters.

### 2.2. Atmospheric exposure

With respect to atmospheric corrosion, *primary parameters* can be defined based on the standard dose response function for atmospheric corrosion (ISO 9233, 2010):

$$C_{\text{corr}} = f(T, \text{RH}, P_d, S_d) \quad (2)$$

Here  $T$  is the air temperature,  $\text{RH}$  is the relative humidity,  $P_d$  is the  $\text{SO}_2$

deposition rate, and  $S_d$  is the chloride deposition rate. The parameters air temperature and relative humidity are considered to define the so-called time of wetness (ISO 9223, 2012; Tidblad et al., 2000). *Secondary parameters* characterize parameters that affect values and distributions of primary parameters. These include precipitation (rain intensity and duration), wind speed, wind direction, and UV radiation. Respective relationships are listed in Table 1. The corrosion models for steel under atmospheric exposure benchmarked in this study are summarized in Appendix A1. Table B1 lists a necessity matrix for the required meteorological sensor parameters.

### 2.3. Immersed exposure

A standard model for *immersed corrosion* in seawater is not available. However, the following *primary parameters* can be considered (Pedeferri, 2018):

$$C_{\text{corr}} = f(T_w, O_2, Cl, v_F) \quad (3)$$

Here,  $T_w$  is the seawater temperature,  $O_2$  is the dissolved oxygen concentration,  $Cl$  is the salinity, and  $v_F$  is the seawater flow velocity. Additional important environmental parameters for immersed corrosion include pH-value, bacteria occupation, and wave action (Melchers, 2002; Melchers and Ahammed, 2006); Respective relationships are listed in Table 1 and in Table 2. The corrosion models for steel under immersed conditions benchmarked in this study are summarized in Appendix A2. The required oceanographic sensor parameters are summarized in Table B2.

A particular aspect of the corrosion under immersed conditions is *cathodic corrosion protection*. The attributes for cathodic protection include basically protection potential (voltage) and protection current density. With respect to DIS ISO 24656 (2020), the following *primary parameters* are assumed:

$$C_{\text{corr}} = f(T_w, O_2, v_F) \quad (4)$$

Here,  $T_w$  is the seawater temperature,  $O_2$  is the dissolved oxygen concentration, and  $v_F$  is the seawater flow velocity. An important parameter for immersed corrosion and cathodic corrosion protection is the specific seawater conductivity, which is, however, related to seawater temperature and salinity. More influencing parameters are listed in

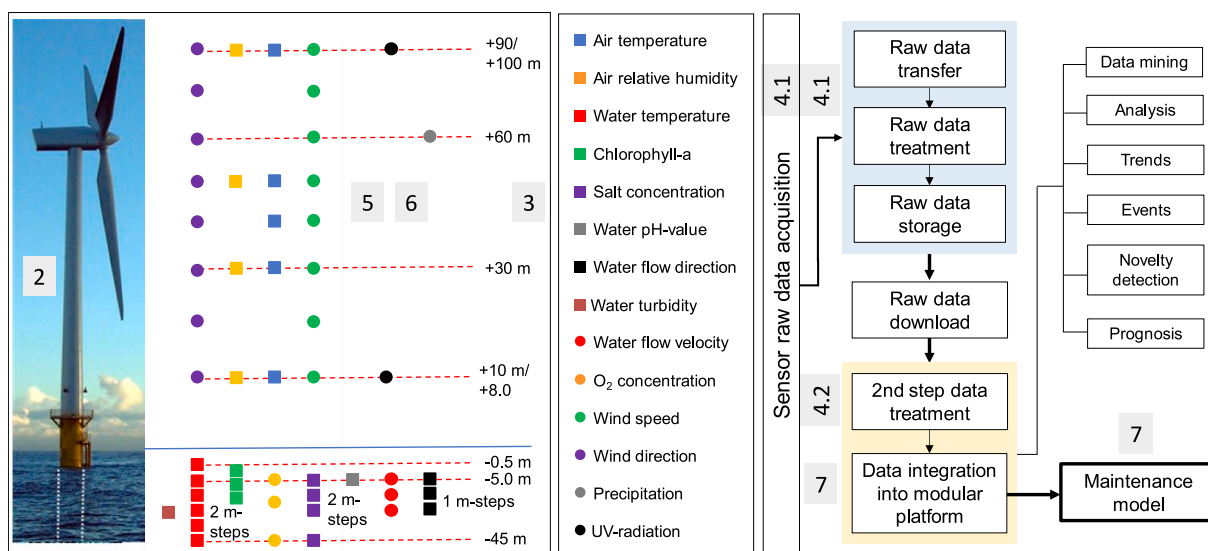


**Fig. 1.** Scope and organization of the paper. The left graph summarizes meteorological and oceanographic sensor data available in the Baltic Sea. The right part illustrates the sensor data treatment. The numbers 2 to 7 refer to the chapters in this paper.

**Table 1**Effects of sensor parameters on corrosion parameters; see [Appendix A](#).

Location	Sensor parameter	Corrosion parameter													
		Chloride deposition	Time of wetness	Wet-dry-cycles	Corrosion rate Eq. (A1)		Localized corrosion	Coating deterioration	Fouling	Cathodic corrosion protection				Microbially influenced corrosion	Electrolyte layer
					Corrosion rate $r_{corr}$	Exponent B				Calcareous deposit	Protection potential	Protection current density	Hydrogen formation		
Atmospheric	Air temperature	X		X	X	X	X							X	X
	Relative air humidity	X		X	X	X	X							X	
	UV radiation	X						X	X	X				X	
	Precipitation	X	X	X	X	X								X	X
	Wind speed	X	X											X	
	Wind direction	X	X					X						X	
	Chloride deposition rate			X	X	X		X						X	
	SO <sub>2</sub> deposition rate			X	X	X									
Immersed	Water temperature			X	X	X	X	X	X	X	X	X	X	X	X
	Water salt content			X	X	X			X	X	X			X	
	Dissolved oxygen			X	X	X		X	X	X	X			X	
	pH-value			X	X	X			X	X	X			X	
	Water specific conductivity			X	X	X			X	X	X			X	
	Chlorophyll							X						X	
	Significant wave height	X	X	X				X			X				
	Water level		X		X		X	X	X	X	X			X	
	Water flow speed			X						X	X			X	

**Table 2**  
Environmental factors in immersed marine corrosion  
(Melchers, 2012).

Factor	Importance
Bacteria	High
Biomass	Low
Oxygen supply	Short-term
Carbon dioxide	Little
Salinity	Not by itself
pH-value	High
Carbonate solubility	Low
Pollutants	Varies
Temperature	High
Pressure	No
Suspended solids	No
Wave action	High
Water velocity	High

[Appendix A3](#) and [Table B2](#). A parameter recently introduced for the design of cathodic protection systems for offshore wind power structures is the *frequently wetted zone* (DIS ISO 24656, 2020):

$$\text{FWZ} = \text{WL} + H_{m0} \quad (5)$$

Here FWZ is the height of the frequently wetted zone, WL is the water level, and  $H_{m0}$  is the significant wave height.

*Fouling* is another considerable factor with respect to the corrosion and corrosion protection of immersed structural parts. A parameter that governs fouling is the chlorophyll concentration in the seawater. Fouling models for steel immersed in seawater are summarized in [Appendix A2](#). [Table B2](#) lists a necessity matrix for the required oceanographic sensor parameters for immersed conditions.

### 3. Environmental sensor networks

In the German offshore territory, the following three networks are installed:

- Marine environment monitoring network (MARNET);
- FINO initiative;
- RAVE initiative.

The locations of the measurement stations and their data transfer methods are marked in [Fig. 2](#). The individual measurement stations are summarized in [Fig. 3](#). Examples for measurement facilities are provided in [Fig. 4](#).

#### 3.1. MARNET

The BSH has installed and runs the marine environment monitoring network (**MARNET**), which covers locations in the North Sea and in the Baltic Sea. MARNET is operated in cooperation with the Leibniz Institute for Baltic Sea Research Warnemünde (IOW) and the German National Meteorological Service (DWD). The locations of the measurement stations are marked in [Fig. 2](#). The monitoring network includes three types of measurement facilities, namely *measurement stations*, *wave buoys* and *costal stations*. MARNET includes sea state measurements and meteorological measurements, as well as oceanographic measurements with measuring chains and bottom-mounted sensors (see [Figs. 3](#) and [4](#)). A review on parameters measured in MARNET, their physical units and their height/depth levels is provided in [Table 3](#) for the North Sea locations and in [Table 4](#) for the Baltic Sea locations.

#### 3.2. FINO

A net of three offshore measurement (research) platforms is available via the initiative **FINO** ("Forschungsplattformen in Nord- und Ostsee"), funded by the Federal Ministry for Economic Affairs and Energy (BMWi), organized by Projektträger Jülich (PtJ), and coordinated by the BSH. FINO includes sea state measurements and meteorological measurements, as well as oceanographic measurements with measuring chains (see [Figs. 3](#) and [4](#)). Locations and sensor data provided by the platforms are listed in [Table 5](#). The meteorological measurements are carried out by UL International GmbH (FINO1), wind-consult GmbH (FINO2), and DNV (FINO3); the data are quality-controlled and made available to the BSH.

#### 3.3. RAVE

When installed in 2009 (opened in 2010), the offshore wind park "alpha ventus", consisting of 12 wind turbines (5 MW) and one transmission platform, was designed as a research wind park. In the frame of the initiative **RAVE** ("Research at alpha ventus"), a number of sensors were installed on four offshore wind power turbines and on the power transmission platform. RAVE is funded by the Federal Ministry for Economic Affairs and Energy (BMWi) and coordinated by the Fraunhofer Institute for Wind Energy Systems (IWES). RAVE includes sea state measurements and turbine measurements (see [Fig. 3](#)). A list of available meteorological and oceanographic sensors is provided in [Table 6](#). The plant and meteorological data are measured by UL International GmbH (turbines AV00, AV07-AV12) and DNV (turbines AV01-

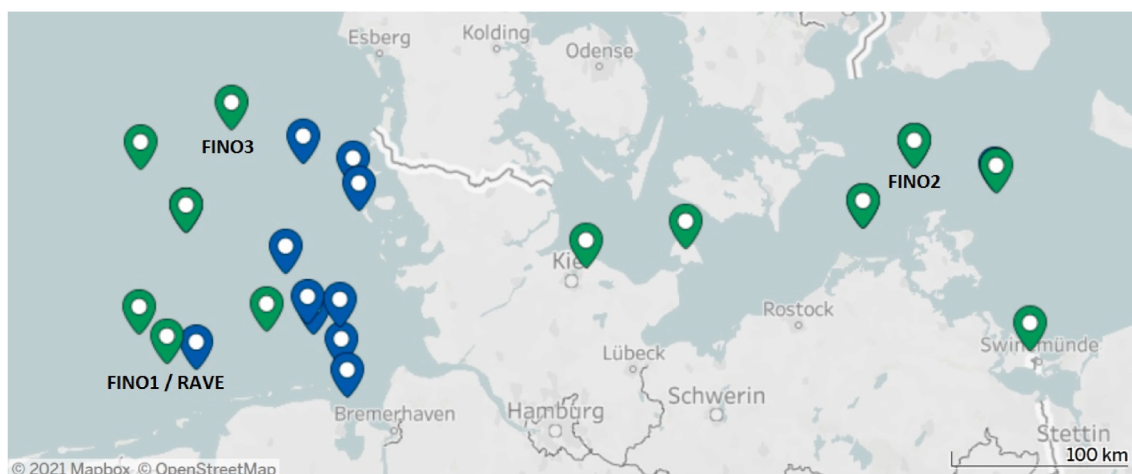


**Fig. 2.** Marine environmental monitoring network MARNET (green marker) and sea state stations (blue marker), including FINO platforms and RAVE offshore wind park "alpha ventus" (modified from BSH, Hamburg). (For interpretation of the references to colour in this figure legend, the reader is referred to the Web version of this article.)

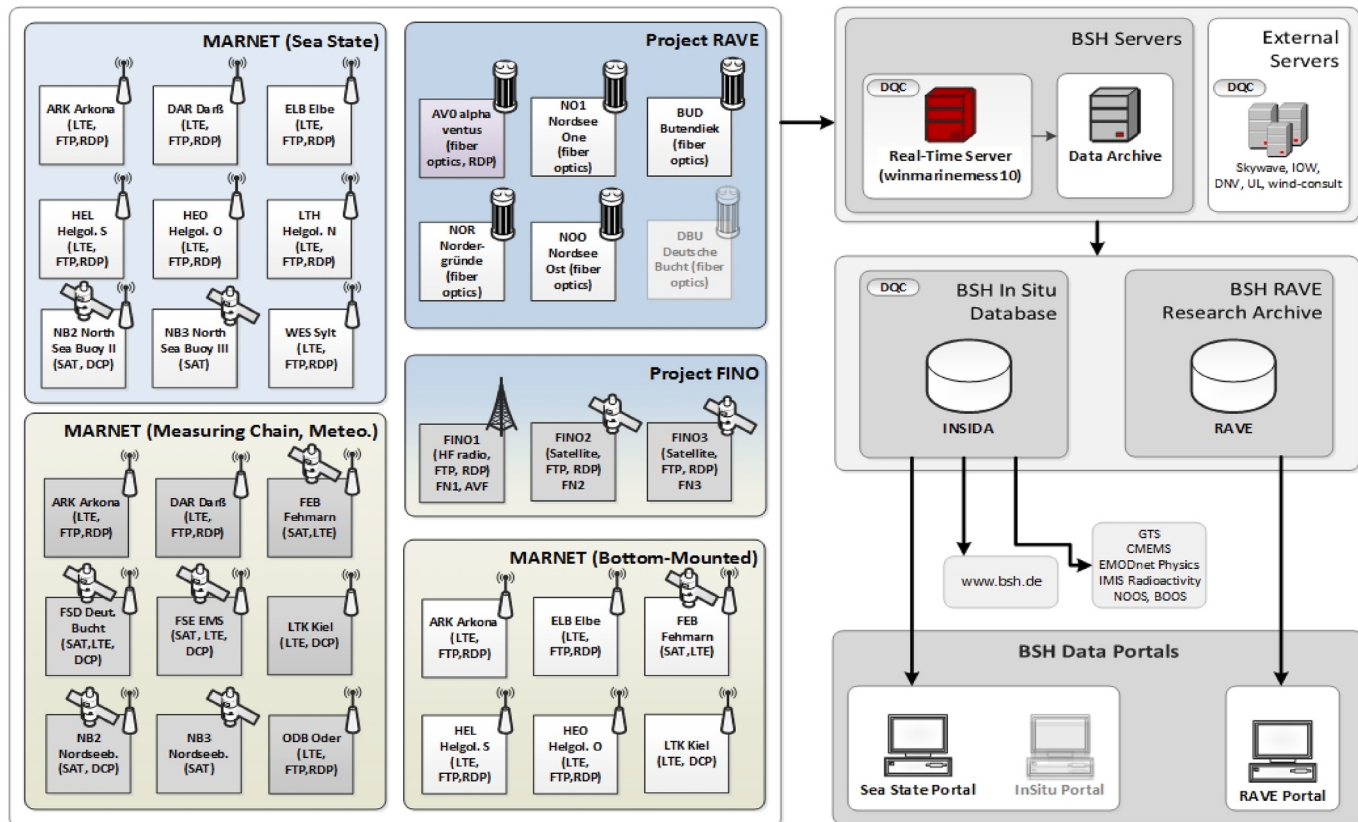


**Fig. 3.** Overview of the measurement stations and their data transfer methods from in situ to the data portals. The meteorological data of the DWD stations are also provided via the DWD's Climate Data Center (<http://www.dwd.de/cdc>).



**Fig. 4.** Measuring station Arkona (left), measuring chain and waverider buoy (middle), bottom-mounted sensors (right); copyright: BSH, Hamburg.

AV06).

Appendix B summarizes the availability of meteorological and oceanographic sensors in the German offshore territory provided by the three networks. Missing solutions (empty boxes) include the sensor-based acquisition of data for the chloride deposition rate ( $S_d$ ), the rain pH-value ( $pH_R$ ), the sunshine duration ( $T_{sun}$ ), the total solar radiation ( $R_{sun}$ ), the nutrition concentration ( $N_C$ ), and for the fouling rate (FA).

#### 4. Data management and treatment

##### 4.1. Raw data from sensors and introduction into databases

###### 4.1.1. Data acquisition, transfer and quality control

The general sensor data treatment chart is shown in the upper section of Fig. 1. The measurement stations and the data transfer to the data portals are illustrated in the flowchart in Fig. 3. The data acquired in the three networks are recorded on the individual station computers (left boxes) and sent via Ethernet/HF radio/mobile broadband/fiber optics, in some cases via satellites (Inmarsat/Skywave), to a shore server, from where they are subsequently pulled to their respective servers. Formats

**Table 3**  
Sensor data from MARNET in the German North Sea.

Parameter	Measurement station													
	Helgoland Nord	Nordseeboje III	Nordseeboje II	Butendiek	Bunker Hill 1	Sylt	FS Deutsche Bucht	Nordsee One	FS Ems	Helgoland RM	Helgoland Süd	Helgoland Ost	Borkum	Elbe
Location	54°13,12'N 07°49,15'E	54°40,95'N 06°45,28'E	54°59,88'N 06°21,08'E	55°47,30'N 07°47,22'E	54°01,48'N 08°13,30'E	54°55,00'N 08°13,30'E	54°10,73'N 07°27,66'E	53°59,11'N 06°50,32'E	54°09,93'N 06°20,78'E	54°10,68'N 07°53,58'E	54°09,55'N 07°52,06'E	54°12,03' N 08°06,05' E	53°33,42' N 06°44,88' E	53°59,79' N 08°07,04' E
Water temperature (°C)	-0.5 m -2.0 m to -35 m	-2.0 m to -35 m	-3.0 to -35 m	-0.5 m	-0.5 m	-0.5 m	-3.0 to -30 m	-0.5 m	-3.0 to -30 m	-1.0 m	-25 m	-25 m	-1.0 m	-25 m
Significant wave height (m)	0 m	0 m	0 m	0 m	0 m	0 m	-	0 m	-	-	0 m	0 m	-	0 m
Relative air humidity (%)	-	10 m	10 m	-	-	-	8.0 m	-	8.0 m	-	-	-	-	-
Air temperature (°C)	-	10 m	10 m	-	-	-	8.0 m	-	8.0 m	-	-	-	-	-
Salt content water (PSU)	-	-6.0 m to -35 m	-6.0 and -35 m	-	-	-	-6.0 and -30 m	-	-6.0 and -30 m	-	-25 m	-25 m	-	-25 m
Oxygen concentration water (ml/l)	-	-6.0 m and -35 m	-6.0 and -35 m	-	-	-	-6.0 and -30 m	-	-6.0 and -30 m	-	-25 m	-25 m	-	-25 m
Chlorophyll (µg/l)	-	-	-	-	-	-	-	-	-	-	-25 m	-25 m	-	-25 m
Turbidity	-	10 m	10 m	-	-	-	15 m	-	15 m	-	-	-	-	-
Wind speed (m/s)	-	10 m	10 m	-	-	-	15 m	-	15 m	-	-	-	-	-
Wind direction (°)	-	10 m	10 m	-	-	-	15 m	-	15 m	-	-	-	-	-
Air pressure (hPa)	-	0 m	-	-	-	-	0 m	-	0 m	-	-	-	-	-
pH-value	-	-6.0 m	-	-	-	-	-	-	-6.0 m	-	-25 m	-25 m	-	-25 m

**Table 4**

Sensor data from MARNET in the German Baltic Sea.

Parameter	Measurement station				
	Darßer Schwellen	Arkona Becken	Oderbank	Fehmarn Belt	LT Kiel
Location	54°41,86' N 12°41,97' E	54°52,9' N 13°51,5' E	54°4,53' N 14°9,49' E	54°35,89' N 11°08,96' E	54°29,98' N 10°16,42' E
Water temperature (°C)	-2.0 m to -21 m	-0.5 m to -45 m	-3.0 m to -12 m	-1.0 m-28 m	-0.5 to -13 m
Significant wave height (m)	-	0 m	-	-	0 m
Relative air humidity (%)	9.0 m	10 m	8.0 m	8.0 m	31 m and 34 m
Air temperature (°C)	9.0 m	10 m	8.0 m	8.0 m	8.0 m and 31 m
Salt content water (PSU)	-2.0 m to -19 m	-2.0 m to -43 m	-3.0 m and -12 m	-3.0 m to -28 m	-4.0 to -13 m
Oxygen concentration water (ml/l)	-7.0 m and -19 m	-7.0 m and -40 m	-3.0 m and -12 m	-6.0 m and -28 m	-8.0 and 13 m
Wind speed (m/s)	9.0 m	10 m	10 m	8.0 m	34 m
Wind direction (°)	9.0 m	10 m	10 m	8.0 m	34 m
Air pressure (hPa)	0 m	0 m	0 m	0 m	0 m
Chlorophyll A (µg/l)	-2.0 m and -5.0 m	-2.0 m and -5.0 m	-3.0 and -12 m	-	-6.0
Solar radiation (W/m²)	9.0 m	10 m	10 m	-	-

**Table 5**

Sensor parameters from the initiative FINO measurement platforms.

Measurement platform	Sensor parameter									
	Global radiation (W/m²)	UV-a-radiation (W/m²)	UV-b-radiation (W/m²)	Air temperature (°C)	Precipitation (yes/no)	Relative air humidity (%)	Water flow direction (°)	Salt content water (ppm)	Water flow velocity (m/s)	Water temperature (°C)
FINO 1 N 54°00,86' E 6° 35,26' (North Sea)	34 m/S/W 93 m/180° 33 m, 90 m	60 m 60 m/180°	60 m 60 m/180°	30, 40, 50, 100 m	20, 90 m	33, 40, 70 90 m	2-30 m (2-m steps)	6, 25 m	2-30 m (2-m steps)	3, 6, 10, 15 20, 25 m
FINO 2 N 55°00,42' E 13°09,25' (Baltic Sea)	60 m/180° 60 m	60 m 60 m/180°	60 m 60 m/180°	30, 40, 50, 99 m	60 m/0°	30, 50, 99 m	2-19 m (1-m steps)	2-20 m (2-m steps)	2-20 m (1-m steps)	2-20 m.(2-m steps)
FINO 3 N 55°11,7' E 00°7'09,5' (North Sea)	29 m/180°	-	-	29, 55, 99 m	22(24) m 95 m/45°	29, 55, 95 m	2-22 m (2-m steps)	6, 12, 18	2-22 m (2-m steps)	6, 12, 18 m

**Table 6**

Sensor parameters from the initiative RAVE at the North Sea offshore wind park "alpha ventus".

Location	Sensor parameter	Level	
		Geographic location	
		54°00,0'N; 06°34,4'E/54°01,6'N; 06°34,4'E 54°01,6'N; 06°37,3'E/54°00,0'N; 06°37,4'E	
Atmospheric	Air temperature (°C)	30/40/50/70/100 m	
	Global radiation (W/m²)	30 m and 90 m	
	Precipitation (yes/no)	20 m and 90 m	
	Relative air humidity (%)	30/50/90 m	
	Air pressure (hPa)	20 m	
	Wind velocity (m/s)	30 m-100 m (10 m-steps)	
	Wind direction	30/50/70/90 m	
	Significant wave height (m)	0 m	
Immersed	Seawater salt content	-10 m and -22 m	
	Oxygen concentration water	-10 m and -22 m	
	Seawater flow direction	4.0 m-30 m (2-m steps)	
	Seawater flow velocity (m/s)	4.0 m-30 m (2-m steps)	
	Seawater temperature (°C)	-29 m	
	Water pressure	-	

include DCP (data compression protocol), LTE (long term evolution), FTP (file transfer protocol), and RDP (remote desktop protocol).

To ensure *data quality*, all oceanographic sensors are calibrated in the calibration laboratory of the BSH or IOW. Regular maintenance trips to the stations are scheduled to clean the sensors from biofouling and to carry out comparative measurements. Errors can thus be corrected subsequently if necessary.

The measuring chain and bottom-mounted sensors (see Fig. 4) log every 10 min on the station computer. Their data, including ADCP (Acoustic Doppler Current Profiler) data, are summarized hourly into a bulletin to be sent afterwards to a central server at the BSH. The bulletin contains the last recorded measured values. The remaining measured values are transmitted via mobile broadband if it is available, or they are reloaded into the BSH server later after a backup at the station.

The directional waverider buoys (DWR; see Fig. 4) log every 30 min on the station computer, and the data are available as 30-min aggregated data. The wave radars (RADAC) log every 1 min on the station computer, and the data are available as 20-min aggregated data. The sea state data are sent half-hourly to the BSH server. Since the bandwidth on the FINO stations is limited, data of the important parameters only are sent in the half-hourly or hourly interval. The complete data set of the day is transmitted once at night. During each maintenance trip, the oceanographic data are backed up to external media, as some data sets are too large for live transmission to the BSH. They are then stored into the BSH server.

The *meteorological data* and plant data are available as 10-min aggregated data. The sensitive plant data (SCADA, Supervisory Control and Data Acquisition) are available as 0.1 Hz aggregated data. For access to the high-resolution 50 Hz sensitive plant data, consent from the manufacturers is required. The data are stored on station computers and

transmitted to their shore servers, from where the respective measuring institutes retrieve their data.

The *oceanographic data* are automatically checked and flagged with the checks recommended by COPERNICUS ([Eurogoos, 2010](#)) during the import into the BSH in-situ database (InSiDa). The checks include date test, station test, completeness test, spike test, range test, stationary test, and comparison against climatology. In a next step, the measured values are checked against comparative measurements and, if necessary, manually corrected. The verified annual data sets of the measuring chain stations are delivered to the German Oceanographic Data Center (DOD) at the BSH and can be requested from there.

The *sea state data* receive an in-depth quality control check (BSH, [2021](#)), performed automatically on the BSH server before they are imported into the BSH InSiDa. The aggregated data are checked following the COPERNICUS standard ([Copernicus, 2020](#)). The raw data (heave and spectrum) are checked following recommendations by [IOOS \(2019\)](#), [Christou and Ewans \(2014\)](#), [Baschek and Imai \(2011\)](#) and [SEADATANET \(2010\)](#).

The *meteorological data* are measured and checked by the respective measuring institutes (DWD, IOW, UL, WIND-consult, DNV) and then transferred to the BSH, where they are imported into the database. As part of the research project FINO-WIND ([Leidig et al., 2016](#)), an automated control routine called „validatf“ is developed and applied to all meteorological data. The automatically controlled data are available in near real time in the DWD Portal and the BSH Insitu Portal. For the FINO stations, the automatic control is followed by a manual data control. Due to the time-consuming visual inspection, the quality-controlled data are sent to the BSH every 1–3 months, where they are immediately automatically loaded into the BSH InSiDa. For the meteorological data, the data quality types listed in [Table 7](#) are applied.

The RAVE sensors deliver basic statistical information (mean, standard deviation, minimum and maximum measured values); examples are provided in [Fig. 7](#). The “alpha ventus” *plant data* are checked by the measuring institutes UL and DNV via automatic controls and a subsequent visual inspection. Formal quality tests include the tests: length, flat line, partial flat line, measurement range, spike counting, correlation, visual evaluation. The automatic control has been extensively expanded within the research project RAVE Offshoreservice (BSH, [2020](#)) and now includes: data set length test, flat line test, range test, spike test, visual control. The quality-controlled data are provided to the BSH on a quarterly basis and imported into the RAVE database. The data quality is ranked as follows: 0 - no event found; 1 - event found; 9 - test not conducted (BSH, [2021](#)).

#### 4.1.2. IT data platform structure (conventions and data format)

Sensor data from the measurement stations are stored into the BSH in-situ database (InSiDa) and will be made available through the BSH Insitu Portal ([Fig. 3](#)). InSiDa uses common international oceanographic standards (OceanSITES, COPERNICUS, SeaDataNet). The metadata of

**Table 7**

Data quality types for meteorological data from the FINO measurement stations (BSH, Hamburg).

Flag	Condition	Comment
9	Missing	No data available
0	Not checked	Not subject to validation
2	Formal pass	Data within sensor limits
2	Climatological pass	Data within climatological limits
3	Time consistency pass	Time series is continuous
3	Internal consistency pass	Good agreement between adjacent sensors
4	Manual pass	Manual override of validate fail flags
1	Manual questionable	Manual check - value considered questionable
5	Formal fail	Data exceeds sensor limits
5	Climatological fail	Data exceeds climatological limits
6	Time consistency fail	Time series is discontinuous (large jumps)
7	Internal consistency fail	Large discrepancy between adjacent sensors
8	Manual fail	Sensor faulty - value known to be wrong

the measurement stations contain international WMO codes, and the parameter labels use COPERNICUS, SeaDataNet and ODV (Ocean Data View) compliant identifiers. Thus, all data are available in a uniform and standardized way after processing. Currently, users receive the data on request, via FTP-server (File Transfer Protocol) or via e-mail. Also, InSiDa data are made available through the BSH North West Shelf Data Portal, CMEMS In Situ TAC (Copernicus Marine Environment Service in situ Thematic Assembly Center), and EMODnet Physics (European Marine Observation and Data Network Physics). Part of the real-time data are fed into the Global Telecommunication System (GTS) network, from which it can be extracted by public institutions that have access to this communication system. A GTS bulletin is generated by adding special header data (time stamp, a sequential numbering, and the official station identification) to the data records (ASCII format). On the BSH website, the data can be plotted, and selected sea state statistics can be retrieved.

The complete, quality-controlled *sea state parameters* and extensive sea state statistics are exclusively available in the specialist application Sea State Portal only. The InSitu Portal and RAVE Portal contain, as sea state data, solely the classic parameters significant wave height, peak wave period, mean wave period, upcrossing wave period (only InSitu Portal), peak wave direction, and maximum wave height.

The measurement data from “alpha ventus” (RAVE), except hydrography, are confidential and only accessible after signing a data use agreement. Therefore, these data are stored in the BSH RAVE research archive and made available via the BSH RAVE Portal. As export file formats, NetCDF (Network Common Data Format) and CSV (Comma-separated values) are possible.

#### 4.2. Management of data from network data portals (2nd step data treatment)

##### 4.2.1. Challenges and data management steps

Challenges associated with the utilization of the data from the BSH data portals (even after raw data management) and their integration into monitoring and maintenance models include the following:

- large amounts of data (several Terabyte per year);
- small trials (trend indications) are very time consuming;
- different/diverse measurement intervals (clock rates between 0.0005 and 200,000);
- different/diverse signal formats;
- missing, inconsistent or defective data (see [Figs. 7 and 16](#));
- data import and management are extremely time consuming;
- standard tools for data analysis fail;
- data are partly unsuitable for machine learning processes;
- data import, treatment and analysis need to be automated.

In order to more efficiently analyze and visualize the data, the following data management measures were performed:

- data acquisition and transfer;
- data cleansing;
- data standardization;
- data storage.

##### 4.2.2. Data pre-processing

Since the sensor data characterized in the previous section come from different sources, numerous collateral problems appear, because measurement intervals and data formats differ greatly between the systems (see [4.1.1](#)). In numerous cases, data are either missing (zero values; see [Figs. 7 and 16](#)) or defective (off the charts values), or data need to be corrected. Moreover, timestamps are off (wrong time zone, clock not set, daylight savings), and data units are diverging (units, formatting, decimals; see [4.1.1](#)). Furthermore, file and stream formats are not standardized and vary greatly. These factors make the management and import of data extremely time consuming and require a



**Fig. 5.** Raw sensor data (lower graphs), treated sensor data (upper graph), and trend analysis for seawater salt concentration and seawater temperature at 6 m water depth after 2nd step data treatment (FINO 1). The lower graphs display the data downloaded from the BSH server. (See Fig. 24 for the relative humidity sensor data.).

smart data preprocessing pipeline. In order to overcome these problems, a high-performance application *Table Transformer* is implemented (see Appendix C). The *Table Transformer* allows for the definition of arbitrary pre-processing steps in a desktop application, that can be applied on any file or data stream, delivering a clean and uniform dataset as a result. Operations possible in *Table Transformer* include the following: reformatting, reordering, filtering, joining, computing, and splitting of sensor data from different sources (e.g. CSV or XML). The user-defined pre-processing steps are stored as a program, that can be run in batch-mode on a server to continuously preprocess incoming data, thus delivering a clean dataset in a fully automated process. Respective screenshots are provided in Appendix C for relative humidity (RH) sensor data from a North Sea location (FINO1, 70 m height). Figure C1 illustrates the selection of input data, whereby lines with useless data are omitted. The correction/formatting of time stamps is shown in Fig. C2: the text is interpreted as calendar date. Uniform data formatting is indicated in Fig. C3; this include decimal separator, thousand separator, and decimal place. Fig. C4 reveals the removal of defective/unsuitable data, whereby lines with data between defined maximum and minimum thresholds are kept.

#### 4.2.3. Data storage

A common problem with analyzing and comparing sensor data at a given time is that the sensor reading intervals differ greatly between different sensors, and that database queries on big datasets tend to be very slow. While, for example, an air temperature sensor ( $T$ ) might

acquire a new reading every second, relative humidity (RH) might only be registered every hour. In order to tackle these challenges, all sensor data must be persisted in a specialized database system (compare Fig. 5 with a harmonized granularity of 1 h). A timeseries database system is able to interpolate data for any given time, based on a per-sensor configuration. This allows for analyzing data at arbitrary temporal granularity, which is mandatory for machine learning purposes, where a complete feature-set is necessary for a given point in time. While regular relational database systems struggle at dealing with big amounts of sensor data, a database system optimized for sequential timeseries data is able to deliver the performance needed for dynamic time-range queries, since it can be highly optimized for linear temporal data. *Timescale* is chosen as a database system, because it is able to deal with great amounts of data, while still delivering the performance needed for interactive queries and machine learning purposes (see Fig. 1, upper right section).

#### 4.2.4. Data visualization and machine learning

For analyzing and visualizing sensor data, a dynamic web-platform is implemented. Using the web-interface, different sensor data can be selected and compared over time. Charts are dynamically generated in real-time and allow for small trials and deep dives into the available data, enabling users to find trends and correlations between different sensors. The example provided in Fig. 5 exhibits trends for seawater salt concentration ( $Cl$ ) and seawater flow velocity ( $v_F$ ) in the North Sea (FINO). Both data sets are harmonized for an hourly data frequency

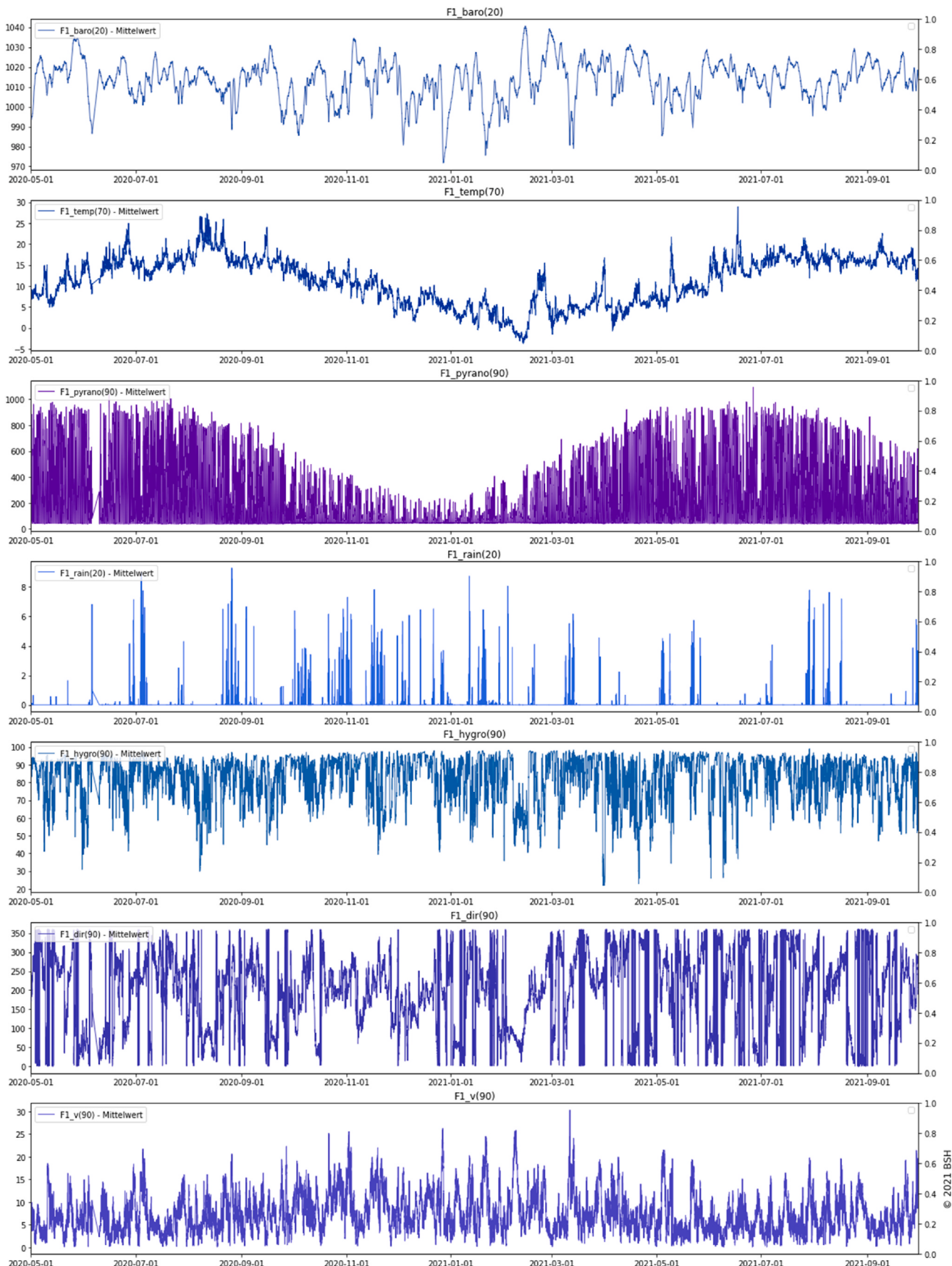


**Fig. 6.** Set of meteorological sensor signals from a North Sea location (RAVE). From top: air pressure (mPa), air temperature (°C), UV radiation ( $\text{W}/\text{m}^2$ ), rain, relative air humidity (%), wind direction (°), wind velocity (m/s).

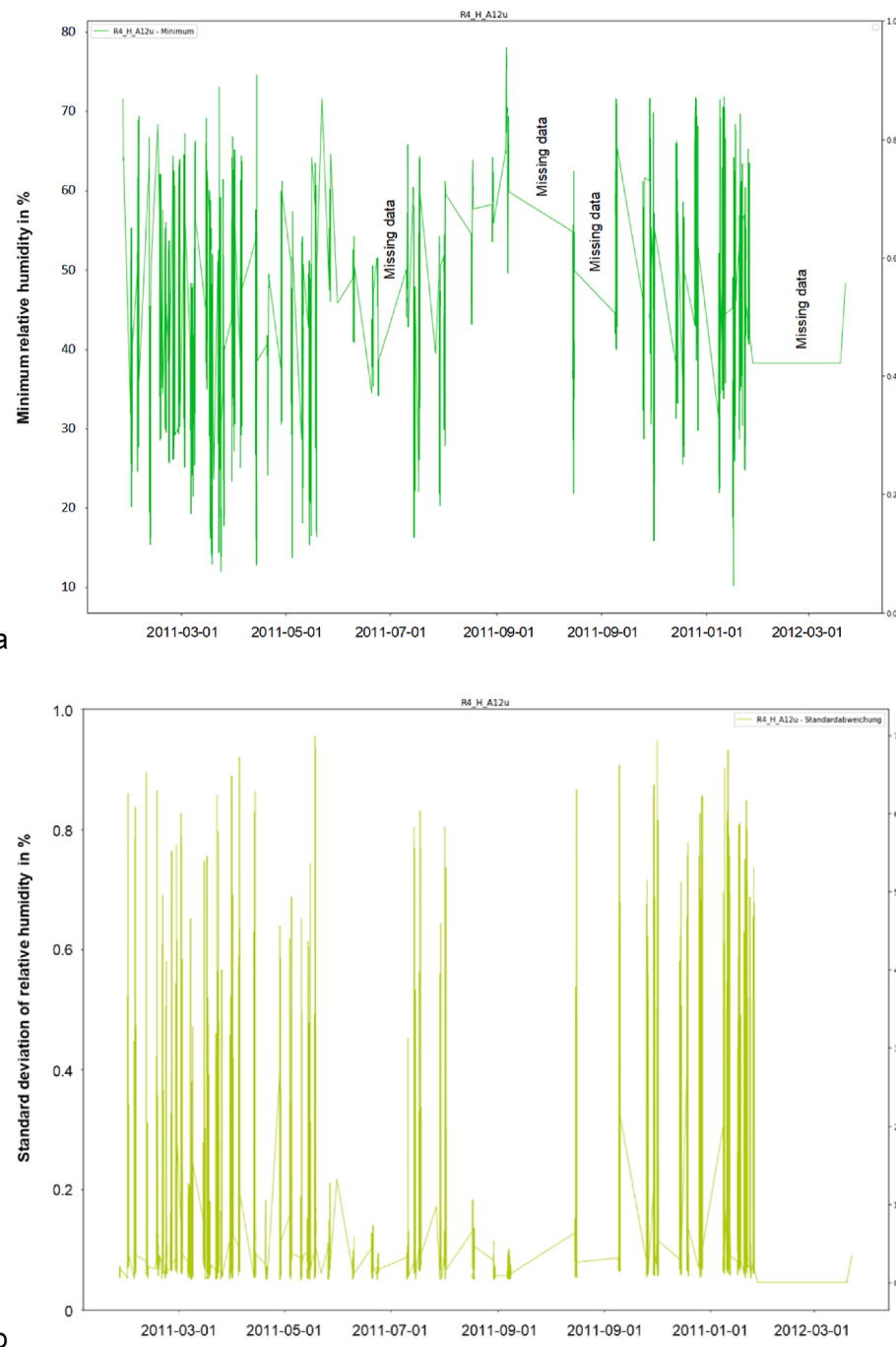


**Fig. 7.** One-year sensor signals for the relative humidity at a North Sea location (RAVE) a - Minimum value. b - Standard deviation.

(granularity). The data layouts, downloaded from the BSH platform, are also provided. Trends, or events, for the two parameters water temperature and salt content can be recognized in the treated data chart only. The sudden drop in either parameter at 08.01. points to a meteorological event. As can be seen in Fig. 24, the relative humidity exhibits a sharp drop at the same day. These trends imply correlations between meteorological parameters and oceanographic parameters (at 6 m water depth), which have not been considered yet in corrosion modeling. The platform also allows the integration of OHLC (Open High Low Close) charts, where initial, highest, lowest and final values are marked.

The system can easily be extended through modules that tie in other data sources that are relevant for a specific use case. An API (application programming interface) for future machine learning processes is established, so that the system can react to certain sensor readings or predict

future developments.

## 5. Selected sensor data

### 5.1. Meteorological sensor data

Fig. 6 contains a set of meteorological sensor data for a North Sea location ("alpha ventus") for a period of 17 months. The data are extracted from the RAVE database. The set contains sensor data for wind direction (WD), air temperature (T), wind speed ( $v_w$ ), relative humidity (RH), UV radiation (UV), rain (P), and air pressure ( $p_a$ ). These signals can characterize the corrosive environment of this particular location. The trends are characterized by a cyclic response, or periodicity; this applies particularly to air temperature, UV radiation (which both exhibit

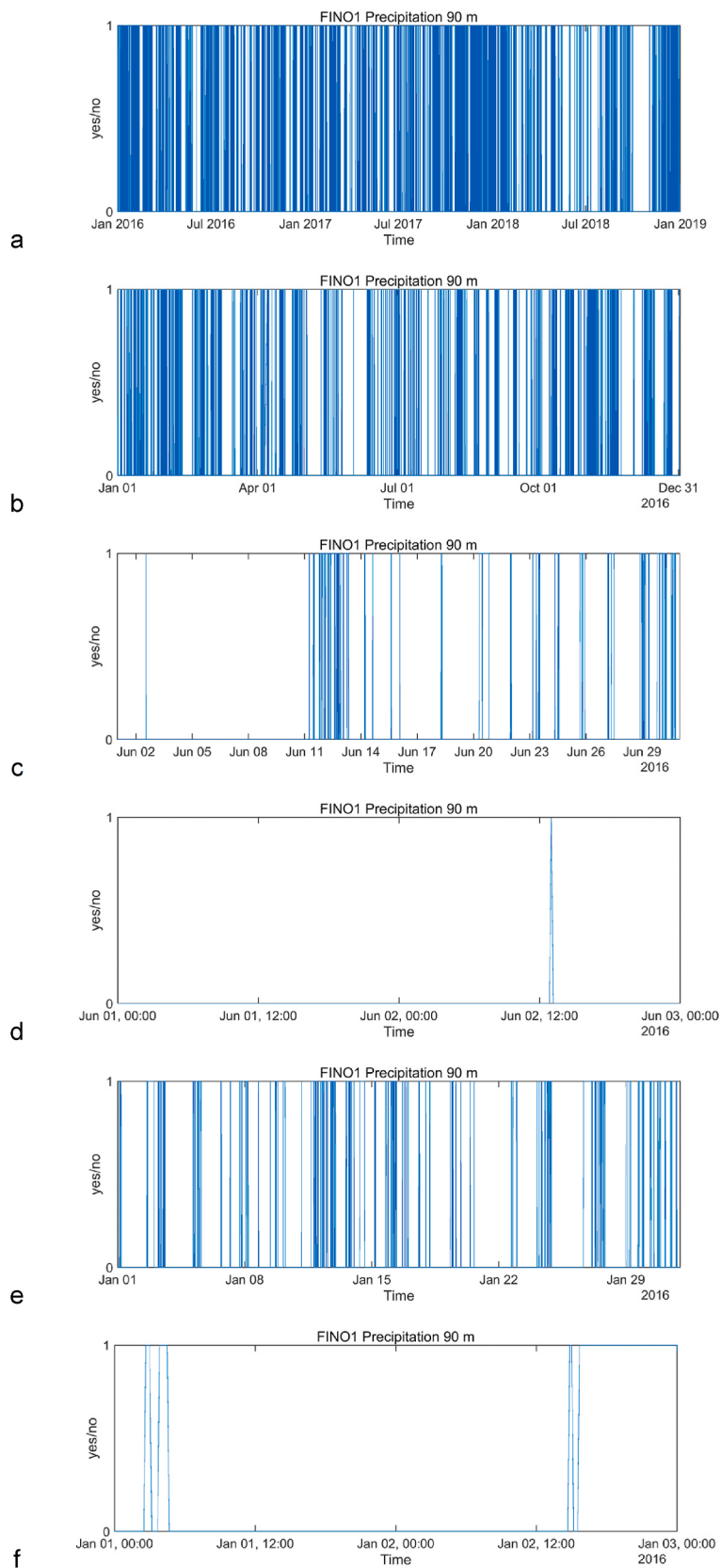


**Fig. 8.** Sensor signals for precipitation at a North Sea location (FINO1) for different time periods and seasons. a - 3-years measurements (153,061 data points). b - 1-year measurements (52,405 data points). c - 1-month measurements (summer, 4321 data points). d - 2-days measurements (summer, 289 data points). e – 1-month measurements (winter, 4465 data points). f - 2-days measurements (winter, 289 data points).

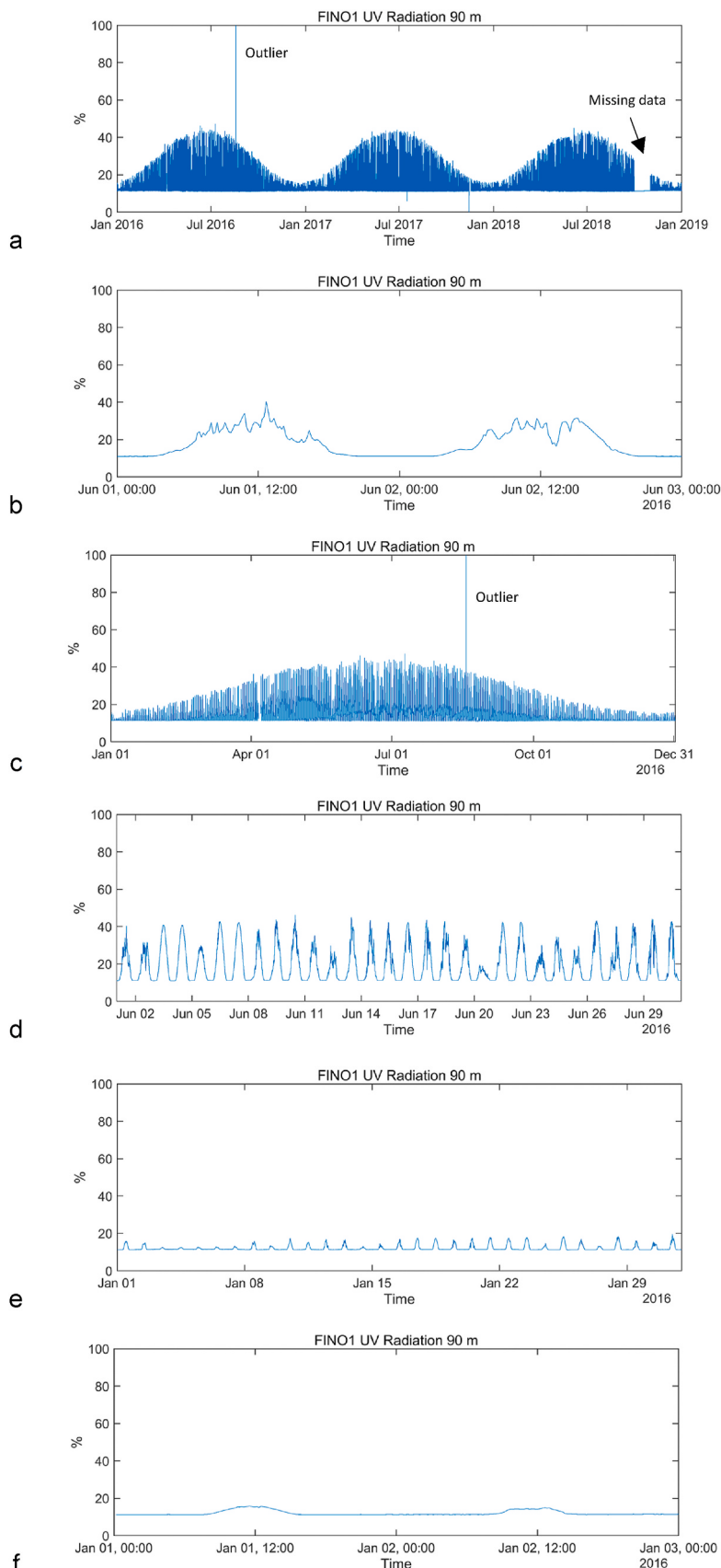


**Fig. 9.** Sensor signals for UV radiation at a North Sea location (FINO1) for different time periods and seasons. a - 3-years measurements (153,360 data points). b - 1-year measurements (52,704 data points). c - 1-month measurements (summer, 4321 data points). d - 2-days measurements (summer, 289 data points). e – 1-month measurements (winter, 4464 data points). f - 2-days measurements (winter, 288 data points).

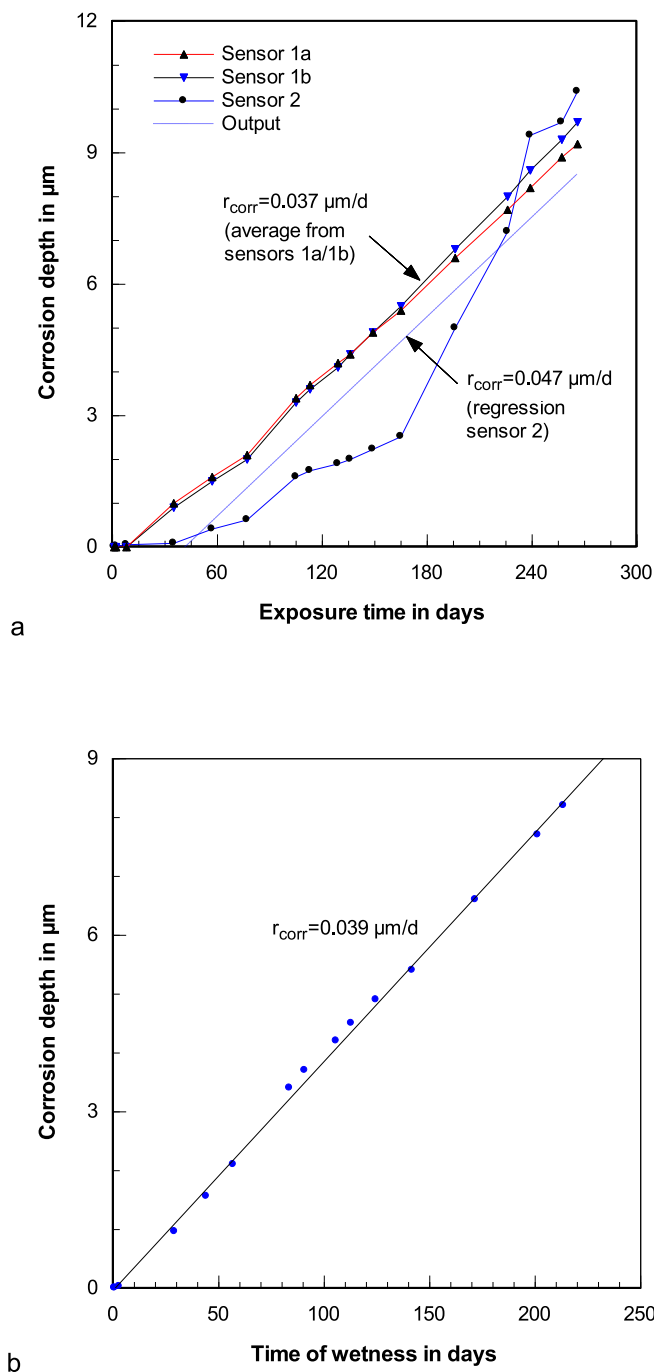


**Fig. 10.** Corrosion sensor signals for a near-shore location (Hamburg, Germany). a - Corrosion depth sensor signals and estimated corrosion rates. b - Correlation between corrosion depth and time of wetness (from sensor 1a/ b data).

equal seasonal trends), and relative humidity. An interesting facet of the signals are the inverse trends between relative humidity and wind speed: relative humidity is low at higher wind speeds, and vice versa. The inverse relationship between air pressure and rainy days is also well documented. (More detailed precipitation sensor data can be found in Fig. 8, and more detailed UV radiation sensor data can be found in Fig. 9.) Fig. 7 shows one-year RAVE signals from a relative humidity sensor (RH), attached to a wind power structure in the North Sea (“alpha ventus”). In contrast to the relative humidity data in Fig. 6, the graphs exhibit values for the *minimum relative humidity* and the *standard deviation* of the measured relative humidity values. The period between

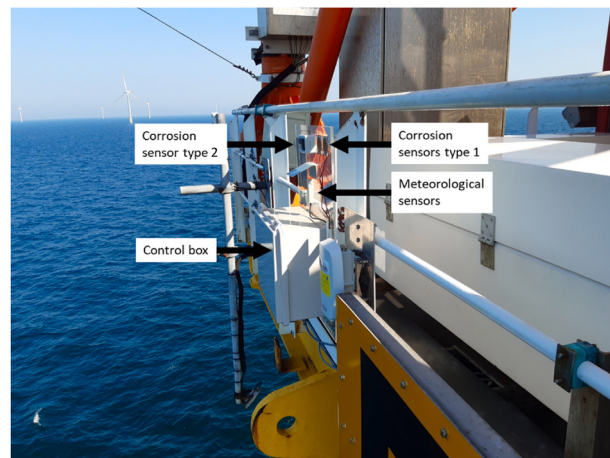


**Fig. 11.** Corrosion sensors and meteorological sensors installations at FINO3 in the North Sea (height: 22 m, direction: Northwest).

August and September is characterized by high minimum values and low standard deviations. The graphs, however, also feature periods with missing data. Precipitation data (P) for a North Sea location, based on 153,061 sensor data, acquired from the FINO network, are plotted in Fig. 8. The graphs illustrate the resolution of the network data, ranging from a 3-years period to 1-day signals. Differences between summer and winter periods can clearly be recognized, with more precipitation events during winter (Fig. 8e). Respective UV radiation data (153,361 sensor data) for the same North Sea location and the same time intervals, acquired from the FINO network, are plotted in Fig. 9. The graphs again illustrate the resolution of the network data, ranging from a 3-years period to 1-day signals. Differences between summer and winter periods can clearly be recognized, with notably higher radiation values during summer. The trends are characterized by a cyclic response, namely in the yearly, monthly and daily resolutions. From the data plotted in Figs. 8 and 9, precipitation is high, and UV radiation is low, during winter, which may contribute to a rather long time of wetness.

All sensor signals discussed above reveal unsteady, partly cyclic or seasonal, trends, and the signals clearly illustrate the need of considering meteorological data [ $Y_1$  in Eq. (1)] as statistically (randomly) distributed data (e.g. Cai et al., 2020).

## 5.2. Corrosion sensor data

In order to specify and to monitor the corrosion term  $h_C(t_E)$  in Eq. (10) in-situ, corrosion sensors were installed on nearshore (Hamburg, Germany) and offshore (FINO 3, North Sea) locations. The signals for the nearshore corrosion sensors are plotted in Fig. 10a. Despite the different electrochemical principles (sensor 1a/b: electrical resistance; sensor 2: current flow), the three sensors reveal comparable trends and deliver comparative corrosion rates between  $r_{\text{corr}} = 0.037$  and  $0.047 \mu\text{m/d}$ . Because the corrosion sensors are coupled with meteorological sensors, the time of wetness could be estimated (based on sensor data for air temperature and relative humidity). Fig. 10b provides a linear relationship between corrosion depth (for sensor 1a) and time of wetness for the early period of corrosion ( $R^2 = 0.998$ ):

$$h_C = 0.039 \cdot \text{TOW} - 0.063 \quad (6)$$

Here, TOW is the time of wetness in days, and  $h_C$  is the corrosion depth in  $\mu\text{m}$ . The function with a power exponent of  $(\text{TOW})^{1.0}$  reveals that no protective corrosion product layer formed over the period of 214 days with wetness, whereby the corrosion process is controlled by oxygen concentration. The sensor installation at the offshore wind platform FINO3 (North Sea) is shown in Fig. 11.

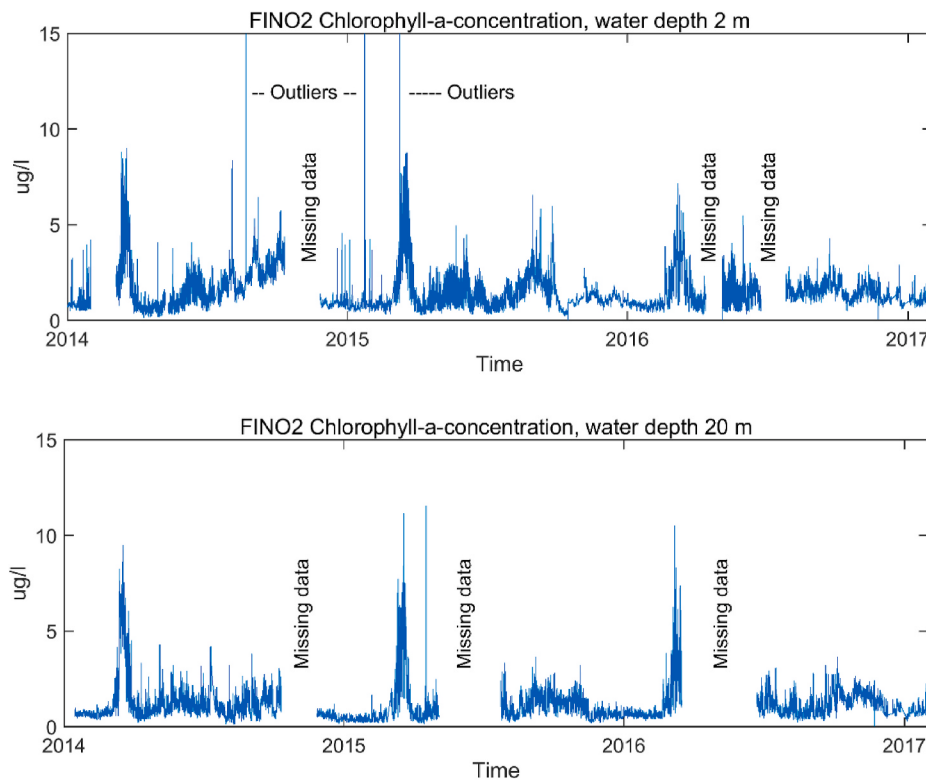


**Fig. 12.** Chlorophyll-a-concentration sensor signals for a location in the Baltic Sea (FINO2) at two water depths (162,205 data points each).

### 5.3. Oceanographic sensor data

Fig. 12 exhibits sensor signals from chlorophyll measurements (Ch) in seawater at two depths in the Baltic Sea (FINO2). The values vary in a wide range between 2 and 13  $\mu\text{g}/\text{l}$ . The chlorophyll concentration is higher in the deeper water (20 m). The signals reveal significant peaks in February/March for either depth. These sensor signals deliver important information for the evaluation of fouling risks; Eq. (A23), (A24). The trends agree with results of Weiss (2011) on “alpha ventus”, who noted most intense fouling in shallow waters, which was attributed to the growth of mussels, and in spring. Fig. 13 shows sensor signals from MARNET for oxygen saturation ( $\text{O}_2$ ) and for pH-values in seawater at different depths in the North Sea for 6 months. The trends for both parameters are equal for 6 m water depth, suggesting a qualitative correlative relationship. Oxygen saturations are notably higher in the shallow water (6 m) for the period between July and September. For the later period, however, the oxygen saturation was independent of the water depth (Fig. 13a). The content of dissolved oxygen in the seawater shows values in excess of 100%, which can be attributed to strong winds and strong wave movement, which could fetch oxygen into the upper water layers (Müller, 2008). The signals for dissolved oxygen notably differ during the two incremental time periods. These signals for  $\text{O}_2$  and pH-values help to predict corrosion rates for steel in seawater [Eq. (A12), (A14), (A15), (A16)] and to design cathodic protection systems (Appendix A3). Short-term seawater salt content (Cl) sensor signals (MARNET) from sensors at two locations and different water depths are displayed in Fig. 14. In the North Sea, the salt content varies between 34 and 35 PSU, and it is independent on the water depth in early February and late March. Between February 10 and March 6, however, the salt concentration is higher in the deeper water (35 m) (Fig. 14a). In the Baltic Sea, the salt content is notably lower and varies in a wide range between 8 and 20 PSU. The salt content is unsteady over time, and it increases with increasing water depth. An event, that reduced the salt content at all water depths (Fig. 14b), happened between 30 November and 4 December. The signals for both situations notably differ during the

respective incremental time periods. The salt content signals help to predict corrosion rates for steel in seawater; Eq. (A15). Fig. 15 provides historical data from MARNET for the seawater surface temperature in April between 1948 and 2017 along with a mean line and a trend line. These data are very helpful to interpret historical corrosion data and corresponding trends. The graph also demonstrates the problems with using mean data; for corrosion modeling, the trend line shall rather be utilized. There is a trend towards higher water temperatures after 1993, although very low temperatures were recorded for some individual years (e.g. 1996 and 2013). Long-term water flow velocity ( $v_F$ ) sensor signals in the North Sea for three seawater depth levels (FINO1) are provided in Fig. 16. The water flow velocities decrease with increasing water depths. There is a tendency towards lower flow velocity in the period 2019–2020. The graphs also illustrate a general problem of sensor data acquisition: missing data (see Section 4.2). The water flow velocity sensor signals help to predict corrosion rates for steel in seawater [Eq. (A13), (A15), (A16)] and to design cathodic protection systems (Appendix A3, Fig. 18). Fig. 17 lists signals for the significant wave height for a 2-months period in the North Sea (RAVE). The graph includes a weather limit of 2.0 m (see Zhang et al., 2021), and the so-called weather days (with no access) can be read. The significant wave height ( $H_{\text{m}0}$ ) sensor signals are particularly important for the calculation of the frequently wetted zone according to Eq. (A22).

The sensor signals shown in Figs. 6, 12, 13 and 14, revealing (incremental) time periods with large variations in meteorological/oceanographic parameters, support the incremental corrosion model of Kovalenko et al. (2017), which may be generalized as follows:

$$r_{\text{corr}} = \int_0^{\Delta t_E} r_{\text{inc}} \left[ \sum_{i=1}^n P_i(t_E), t_E \right] dt_E \quad (7)$$

Here,  $\Delta t_E$  is the time increment,  $r_{\text{inc}}$  is the corrosion rate during the time increment, and  $P_i$  is the respective oceanographical parameter. Incremental time periods  $\Delta t_E$  are marked in the respective graphs. The signals reveal that an incremental approach might be applied for short-term

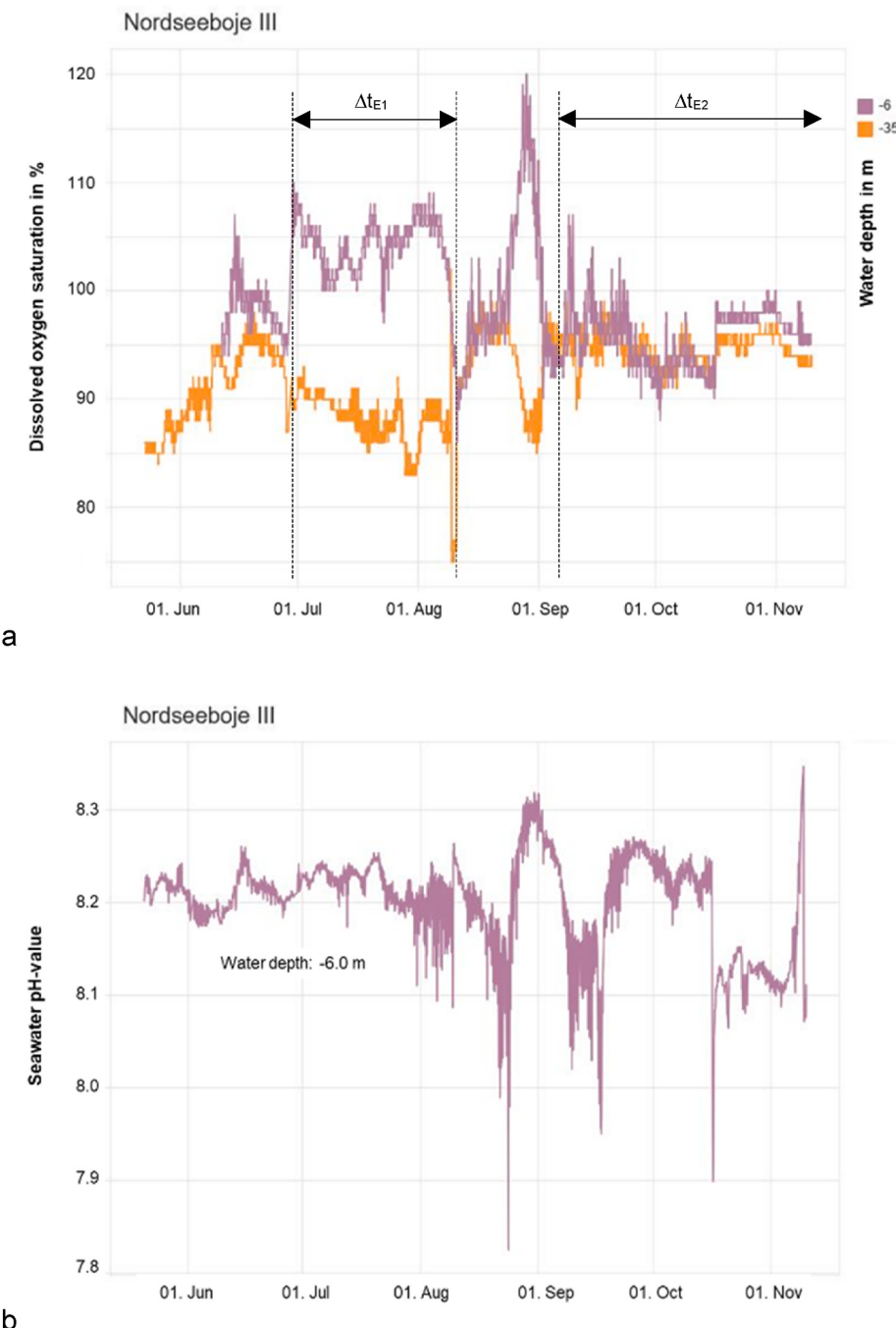


**Fig. 13.** Sensor signals from MARNET in seawater at different depths in the North Sea for 6 months.  $\Delta t_{Ei}$  refer to time increments according to Eq. (7) a - Dissolved oxygen saturation. b - pH-value.

time intervals as well in order to consider the complex unsteady load characteristics of the respective oceanographic parameters.

## 6. Selected applications of sensor data

### 6.1. Time of wetness

The time of wetness is considered a key parameter for atmospheric corrosion (ISO 12944-2, 2018; ISO 9223, 2012; Tidblad et al., 2000, see also Eq. (A5), and it is usually defined as the time with a relative humidity greater than 80% at an air temperature greater than 0 °C (ISO 9223, 2012). Values for the time of wetness, based on this definition, are shown in Fig. 18 for two locations (FINO). The graph values are

calculated from a total of 500,000 sensor data points for air temperature and relative humidity. The time of wetness is notably higher at the North Sea location compared with that at the Baltic Sea, which is basically because of the higher relative humidity. The average air temperatures, in contrast, are almost equal at the two locations. The time of wetness (and the relative humidity) is higher at the lower atmospheric height. A more general definition for the time of wetness is a “*period when a metallic surface is covered by adsorptive and/or liquid films of electrolyte to be capable of causing atmospheric corrosion*” (ISO 8044, 2015). Therefore, the integration of precipitation (moisture) sensor data and UV radiation sensor (drying) data (see Figs. 8 and 9) into the calculation procedure may further improve the results.

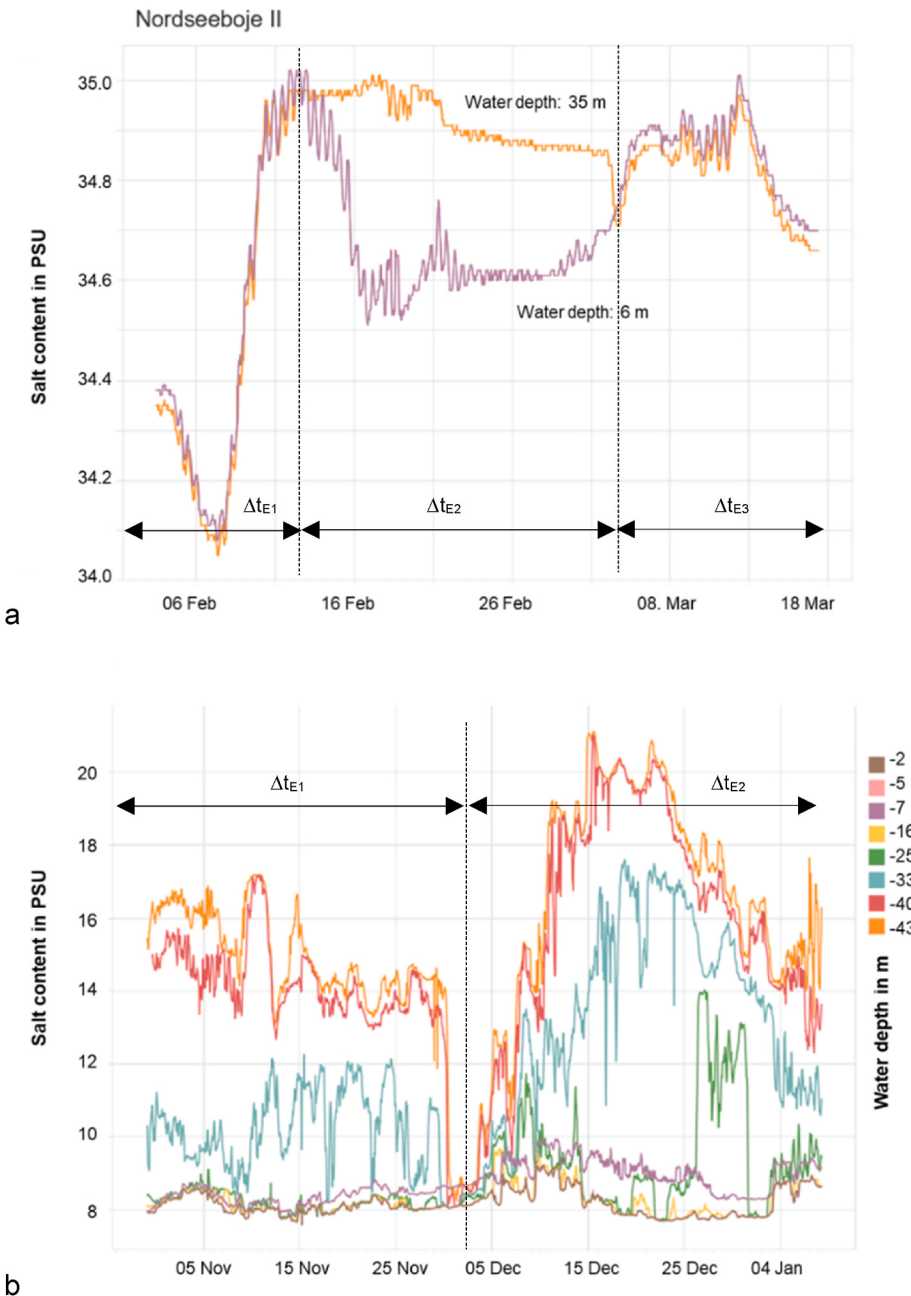


**Fig. 14.** Salt concentration sensor signals for two locations (MARNET).  $\Delta t_{Ei}$  refer to time increments according to Eq. (7) a - North Sea. b - Baltic Sea.

## 6.2. Cathodic protection current density

Fig. 19 is an example for the use of sensor data for the design of cathodic corrosion protection systems for offshore wind power structures, specifically for the relationship between seawater flow velocity and cathodic protection current density. It displays average water flow velocities ( $v_F$ ), calculated from 300,000 sensor data points at different depths in a North Sea location (FINO 1). The trend corresponds to results reported by Hahn et al. (2021) for the period of 2012–2015, and it reflects very well the trend example provided in ISO/DIS 24656 (2020). The sensor data are employed to compute required cathodic protection current densities at different seawater depths according to a procedure outlined in ISO/DIS 24656 (2020) for 10 m-depth increments. As shown in Fig. 19, the current density slightly drops for deeper waters from 67 mA/m<sup>2</sup> to 62 mA/m<sup>2</sup>, which corresponds to a drop of 7.5%.

## 6.3. Frequently wetted zone

Oceanographic sensor data are also used to calculate the height of the frequently wetted zone by means of Eq. (A22). A calculation sample, based on 220,000 sensor data points for the average water level (WL) and the average significant wave height ( $H_m0$ ) in a North Sea location (FINO 1), is illustrated in Fig. 20. The 50-percent quantile of the frequently wetted zone ( $FWZ_{50\%} = 1.10$  m) can be taken as a good estimate of the level to which the structure impacts the mean anode current drain from the cathodic protection system. The 95-percent quantile of the frequently wetted zone ( $FWZ_{95\%} = 2.98$  m) represents the impact of a storm (as a singular event) on the anode current drain (ISO/DIS 24656, 2020). It is for the first time that these parameters have been computed entirely with sensor signal data.

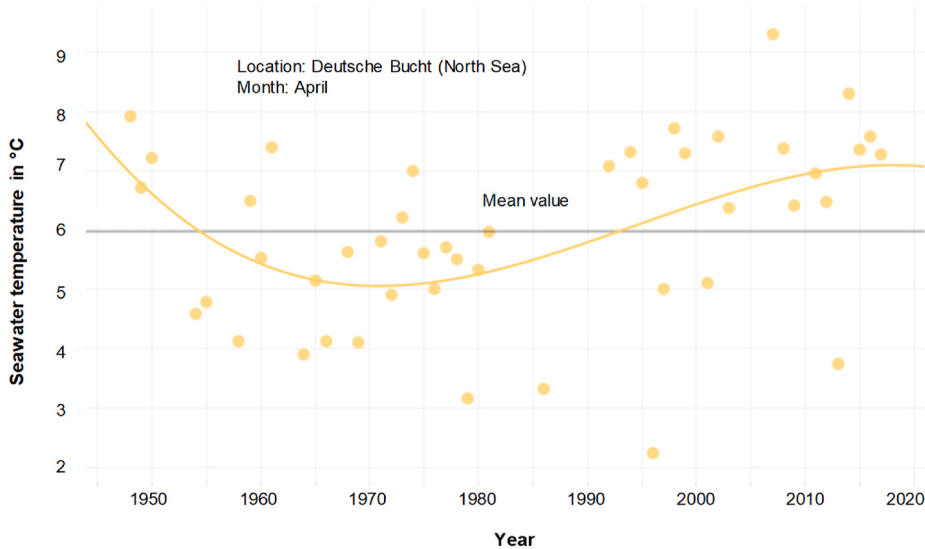


**Fig. 15.** Historical data for the monthly mean value of the seawater surface temperature at a North Sea location (MARNET).

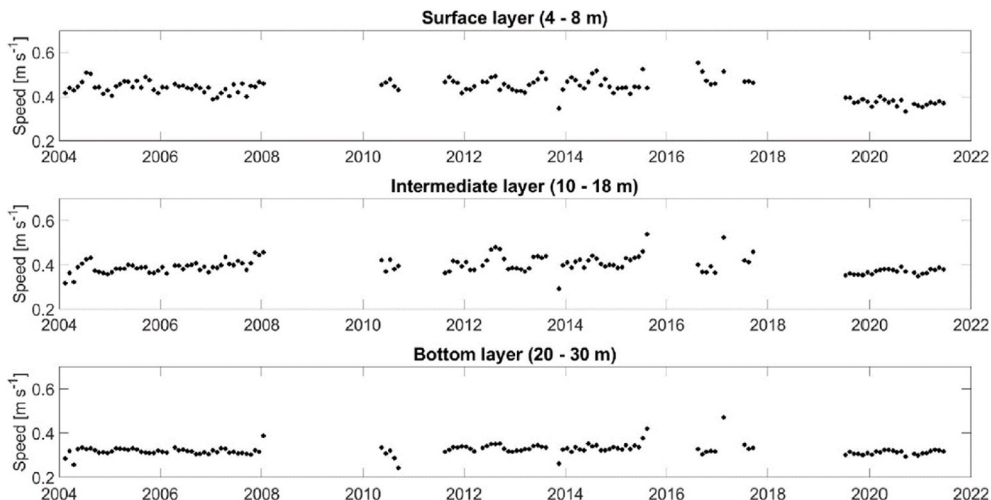


**Fig. 16.** Monthly average water flow velocities, based on long-term sensor data at different water depths (FINO1) (Hahn et al., 2021).

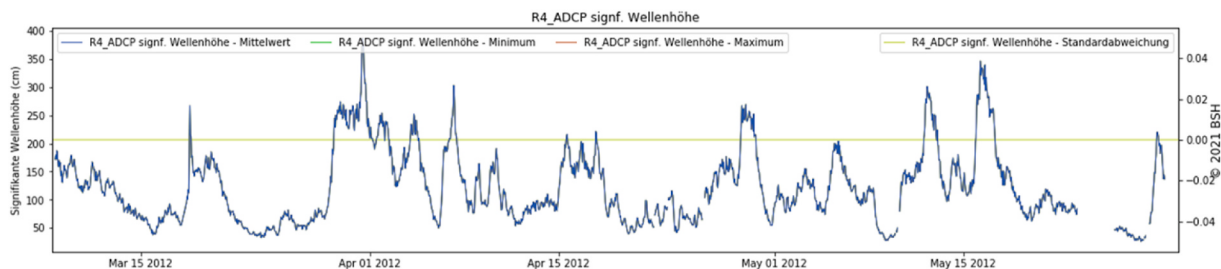


**Fig. 17.** Sensor data for the significant wave height at a North Sea location (RAVE).

## 7. Integration into an online monitoring and maintenance system

### 7.1. Corrosion monitoring and maintenance system

A general approach for maintenance scheduling for the corrosion protection systems on steel structures is proposed by [Momber et al. \(2022\)](#):

$$g(D) = R(t_E) - S \quad (8)$$

Here,  $g(D)$  is the limit-state function,  $D$  is the rating parameter,  $R$  is the time-variant function for the *resistance* effect,  $S$  is the value for the given (constant) *load* effect (critical values at limit state), and  $t_E$  is the operation time. At  $g = 0$ , the surface protection system at the reference area is in the limit state; for  $g < 0$ , the system is in the failure state; for  $g > 0$ , the system is in the survival state. The rating parameter is a local

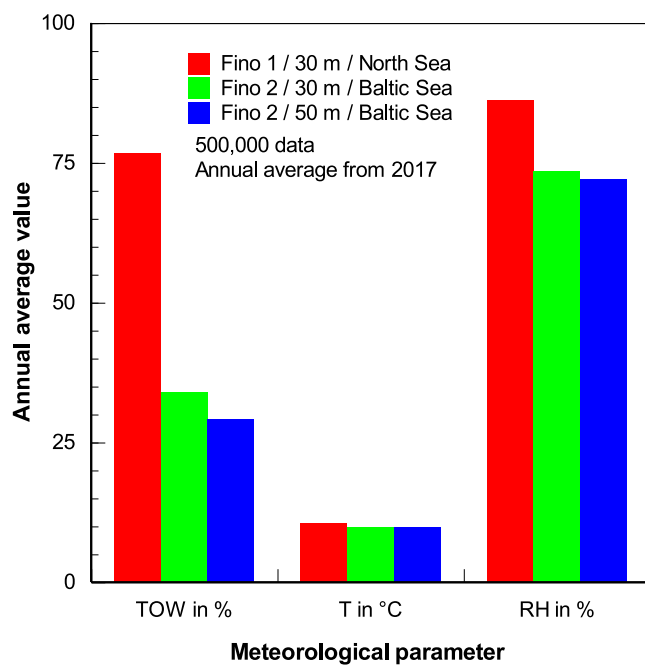


**Fig. 18.** Average values for time of wetness, air temperature and relative humidity at three locations, calculated from 500,000 sensor data points.

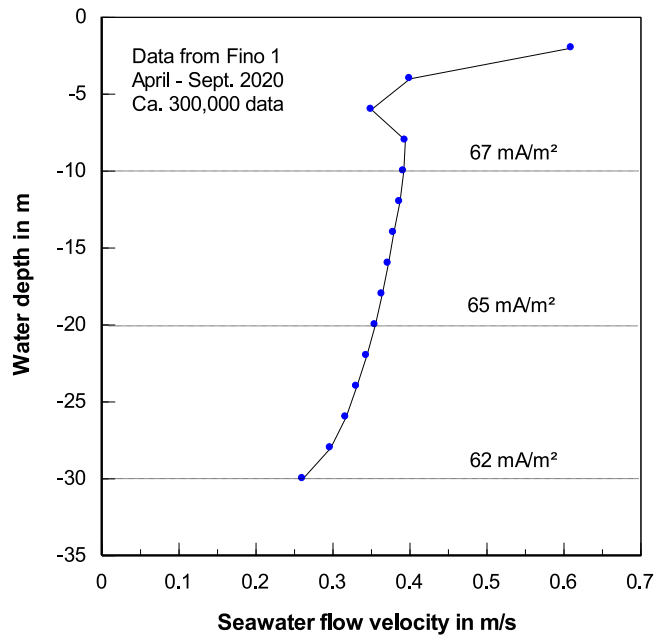


**Fig. 19.** Relationship between water depth and water flow velocity (based on sensor data), including 10-m depth increments (FINO) and estimated average protection current densities according to ISO/DIS 24656 (2020).

deterioration degree, which follows a Weibull-type function (Momber et al., 2022):

$$R(t_E) = D_L(t_E) = \exp \left[ -(\lambda \cdot t_E)^k \right] \quad (9)$$

The analytical solution, however, includes the following subfunctions:

$$R(t_E) = f[R_i(t_E), h_C(t_E), N_C(t_E)] \quad (10)$$

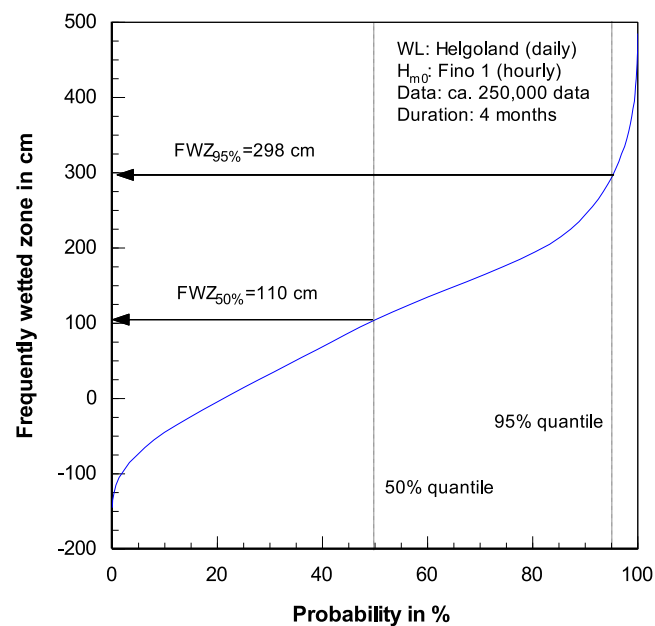


**Fig. 20.** Estimation of the frequently wetted zone for the design of a cathodic protection system (based on sensor data for average water level and average significant wave height) according to ISO/DIS 24656 (2020).

In the equations,  $D_L$  is the local deterioration degree,  $t_E$  is the exposure time in years,  $\lambda$  and  $k$  are scale and shape parameter of the function,  $R_i$  is the degree of paint rusting,  $h_C$  is the corrosion depth for uniform corrosion, and  $N_C$  is the fatigue limit for pitting corrosion. Thus, the local deterioration degree covers three deterioration effects: coating deterioration, uniform corrosion, localized (pitting) corrosion. It takes values between 1.0 (non-deteriorated) and 0 (completely deteriorated). The reader may refer to Momber et al. (2022) for more details. The relationship between meteorological sensor data and the local deterioration degree  $R(t_E)$  is illustrated in Fig. 21 (meteorological sensor data are highlighted). The sensor data are intended to be utilized for the calculation of the corrosion depth  $h_C(t_E)$  and the degree of coating deterioration  $R_i(t_E)$  in Eq. (10), which both determine the local deterioration degree (resistance effect). With respect to Eq. (9), for atmospheric exposure, the following interrelationships were found to apply (Momber et al., 2022):

$$\lambda, k = f[P_d(t_E), RH(t_E), T(t_E), S_d(t_E), UV(t_E)] \quad (11)$$

Data for the environmental parameters  $P_d$ , RH, T,  $S_d$  and UV are attempted to be acquired from meteorological measurement stations in defined time intervals. This is illustrated in Fig. 6, where sensor data for RH, T and UV are plotted. The availability of sensor data is summarized in Table B1. No sensor data are available for the sulfur dioxide deposition rate. Based on data in ISO 9223 (2012), we developed an alternative approach ( $R^2 = 0.998$ ):

$$P_d = 0.892 \cdot SO_2 - 0.869 \quad (12)$$

Here,  $P_d$  is the sulfur dioxide deposition rate in  $mg/(m^2 \cdot d)$ , and  $SO_2$  is the sulfur dioxide concentration in  $\mu g/m^3$  (between 5 and 90  $\mu g/m^3$ ). Sensor data for the latter parameter can be taken either from weather stations or from air quality monitoring networks (e.g. Copernicus); an example is provided in Fig. 22. Sensor data are neither available for the chloride deposition rate. However, alternative solutions are available, namely the use of digital speckle correlation (DSC) for the automatic detection of chloride deposition (in  $\mu g/cm^2$ ) (Horstmann et al., 2015), and the regression of chloride depositions (in  $g/m^2$ ) from atmospheric sensor data (Shinohara et al., 2005). An example for the use of the latter method is illustrated in Fig. 23. A comparison with Fig. 10a reveals a

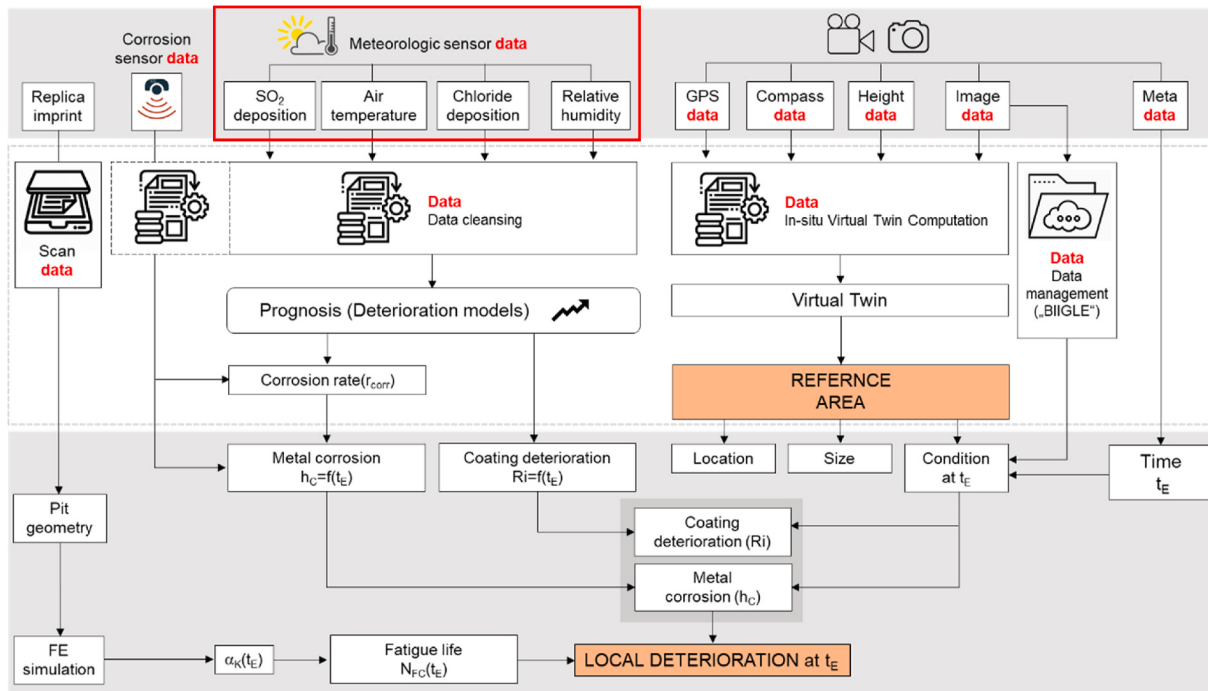


**Fig. 21.** Structure of the data-based monitoring and maintenance concept for atmospheric exposure (Momber et al., 2022). Meteorological sensor data are highlighted (farmed).

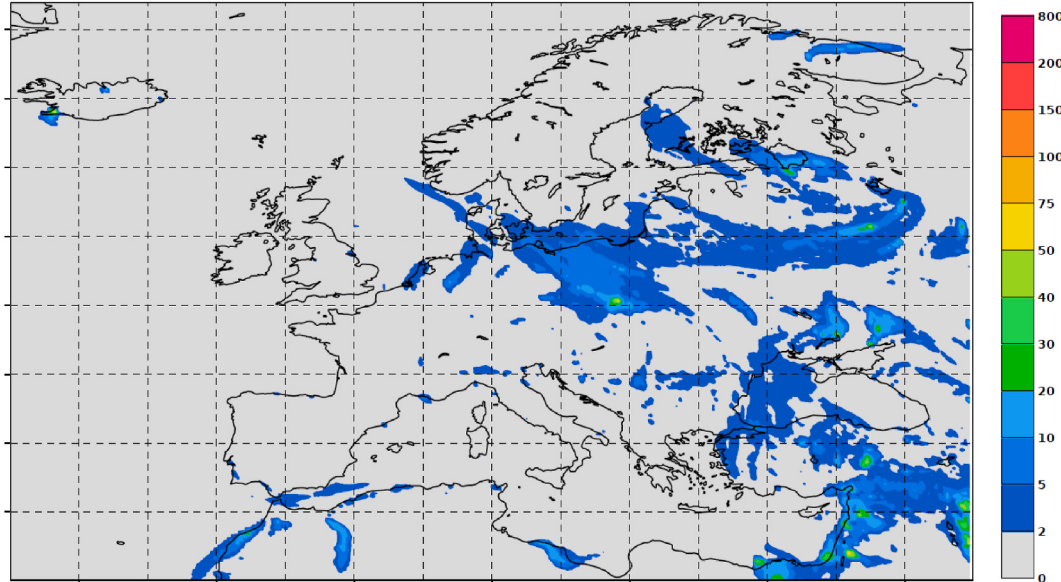


**Fig. 22.** European sulfur dioxide (SO<sub>2</sub> in  $\mu\text{g}/\text{m}^3$ ) concentration map for November 25, 2021 (reference: Copernicus/Atmosphere Monitoring Service).

relationship between chloride deposition and corrosion depth in carbon steel in a sense that high chloride deposition values correlate with high corrosion rates (progress of the curve for sensor 2 in Fig. 10a) after about 200 days.

## 7.2. Integration of sensor data and other data domains into the system

The integration of sensor data into a preventive maintenance system is schematically illustrated in Fig. 1. The modular concept of the web platform introduced in Section 4.2 allows for the integration of inspection reports/data, images of the structure to be analyzed, 3D displays, and fault detection algorithms based on machine learning or manual

annotations. By projecting inspection images onto the structure, thus exactly locating each fault on the structure, a virtual twin of the structure can be computed. As soon as multiple inspections have been conducted over time, the development of damages can be reconstructed and visualized on the virtual twin. These options are illustrated in Fig. 24.

All inspection data are persisted with timestamps alongside the available sensor data, creating an extensive data pool that can be used to expand on temporal correlations between sensor data and damages found in the image data, thus enabling analysts to more accurately predict the deterioration of the structure and update the maintenance system. Because the web platform is open and generic, it can be integrated into other marine asset condition management systems.

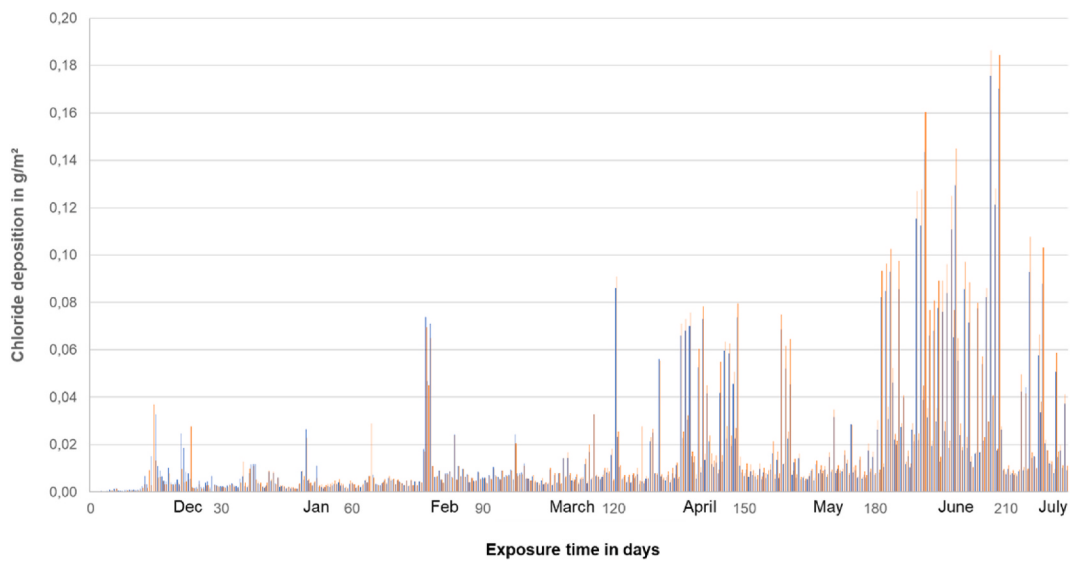


**Fig. 23.** Extrapolated chloride deposition data from meteorological sensor data under atmospheric exposure (Momber et al., 2021b).

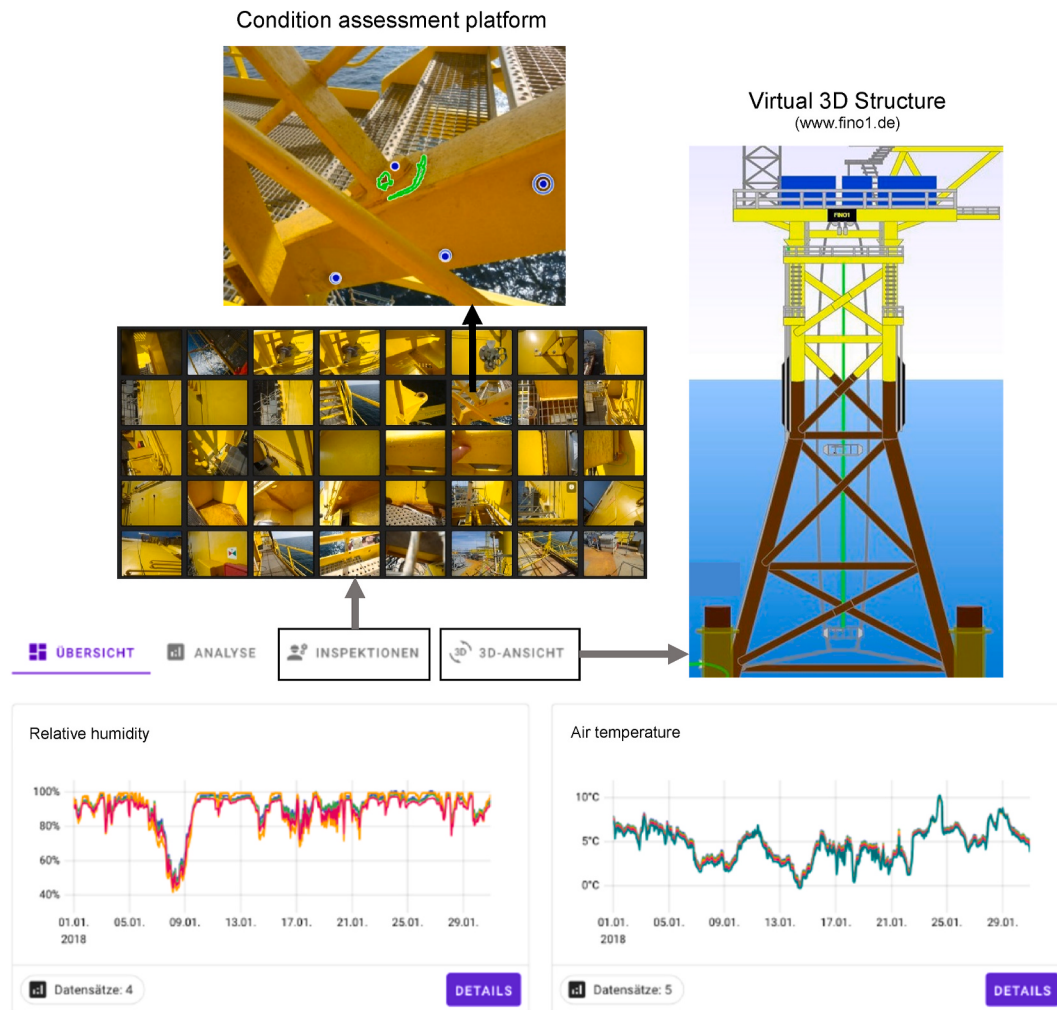


**Fig. 24.** Integration of sensor data (relative humidity, air temperature), virtual structure ("3D-ANSICHT") and condition assessment platform ("INSPEKTIONEN") into the web platform (see Fig. 5 for trends in oceanographic parameters).

## 8. Summary and outlook

The results of the paper can be summarized as follows:

- The requirements for sensor signals/data for the modeling of atmospheric and immersed corrosion processes in marine environments are benchmarked, and sensor necessity matrices are provided.
- Sensor data delivered by three environmental sensor networks in the German offshore territory (North Sea, Baltic Sea) are reviewed and categorized, and sensor availability matrices are presented for the first time.
- Practical problems with data acquisition and processing are discussed, and a 2-step data treatment procedure is introduced.
- Sensor data can be utilized to characterize marine environments, respectively corrosive loads, at different resolutions with respect to location (micro-corrosivity) and time (incremental corrosivity).
- Sensor data can be utilized to treat important practical design issues with respect to corrosion protection, namely to cathodic protection.
- The integration of acquired data into data-based monitoring and maintenance model, and the interconnection with other data domains (visual inspection data) and with virtual structures offer the opportunity to introduce prescriptive maintenance strategies.

## APPENDIX A. CORROSION MODELS

### A1. Atmospheric corrosion

[ISO 9224 \(2012\)](#).

$$h_C = r_{corr} \cdot [20^B + B \cdot (20^{B-1}) \cdot (t_E - 20)] \quad (A1)$$

$$r_{corr} = A \cdot B \cdot t_E^{B-1} \quad (A2)$$

[Feliu et al. \(1993\)](#).

$$B = 0.531 + 0.115 \cdot MAQ + 0.00112 \cdot N_d - 0.221 \cdot TOW \quad (A3)$$

$$MAQ = 1.0 \text{ for } S_d \geq 0.1 \text{ mg/(dm}^2\text{-d)}$$

[Vera et al., 2018](#).

$$r_{corr} = f_{ANN}(P_d, S_d, RH, T, R_f, v_w) \quad (A4)$$

[Kihira et al. \(2005\)](#).

$$Z = \alpha \cdot TOW \cdot \exp \left( -\kappa \cdot v_w \cdot \frac{S_d + \delta \cdot P_d}{1 + \varepsilon \cdot P_d} \cdot \exp \left( \frac{-E}{R_G \cdot T} \right) \right) \quad (A5)$$

[ISO 9223 \(2012\)](#).

$$r_{corr} = A_1 \cdot P_d^{A_2} \exp(A_3 \cdot RH + f_T) + A_4 \cdot S_d^{A_5} \cdot \exp(A_6 \cdot RH + A_7 \cdot T) \quad (A6)$$

[Alcantara et al. \(2015\)](#).

$$S_{d0} = 284.5 \cdot H_w^{1.68} \quad (A7)$$

[Meira et al. \(2008\)](#).

$$S_d = S_{d0} \cdot \exp \left( \frac{v_{dep}}{\alpha_1 \cdot H} \right) \cdot \left[ \exp \left( \frac{-\alpha_1 \cdot X}{v_w} \right) - 1 \right] \quad (A8)$$

[Corvo et al. \(2008\)](#).

$$\Delta W = A \cdot t_E^B \cdot S_d^C \cdot \left( \frac{R_f}{N_d} \right)^D \quad (A9)$$

[Bhaskar et al. \(2004\)](#).

## CRediT authorship contribution statement

**A.W. Momber:** Conceptualization, Calculations, Writing – review & editing. **M. Wilms:** Data curation, Validation, Writing – review & editing. **D. Brün:** Data curation, Data management, Writing – review & editing.

## Declaration of competing interest

The authors declare that they have no known competing financial interests or personal relationships that could have appeared to influence the work reported in this paper.

## Acknowledgements

The project ISyMOO was funded by the Federal Ministry of Economic Affairs and Energy (BMWi) through the 6th National Energy Research Program (grant number: 0324254A-E). FINO data were provided by the Initiative FINO, funded by the Federal Ministry for Economic Affairs and Climate Action (BMWK), organized by Projektträger Jülich (PtJ), and coordinated by the Federal Maritime and Hydrographic Agency (BSH). Thank is addressed to Mrs. Maren Engelhardt, Fraunhofer IWES, Bremerhaven, Germany, for support with the RAVE project.

$$r_{corr} = \sum_{i=1}^4 r_i \cdot c_i \quad (A10)$$

( $i_{1-4} = RH, T, S_d, P_d$ )

## A2. Immersed corrosion

[Garbatov et al. \(2011\)](#).

$$r_{corr} = 0.0014 \cdot T_w + 0.0154 \quad (A11)$$

[Guedes Soares et al. \(2005\)](#).

$$f(pH) = k_r \cdot 10^{-(n \cdot pH)} \quad (A12)$$

[Garbatov et al. \(2011\)](#).

$$r_{corr} = 0.9338 \cdot \{1 - \exp[-0.4457 \cdot (v_F - 0.2817)]\} \quad (A13)$$

$$h_C = 0.0268 \cdot O_2 - 0.0086 \quad (A14)$$

[Pederferri \(2018\)](#).

$$r_{corr} \propto 10 \cdot 2^{\frac{T_w - 25}{25}} \cdot [O_2 + 0.04 \cdot Cl] \cdot (1 + v_F^{0.5}) \quad (A15)$$

[Melchers and Ahammed \(2006\)](#) (corrosion of fixing chains).

$$r_{corr} = 0.056 \cdot \exp(0.065 \cdot T_w) \cdot \frac{O_2}{O_{2B}} \cdot (1 + 4.60 \cdot v_F) \quad (A16)$$

[Khodabux et al. \(2020\)](#).

$$r_{corr} = 1.075 \cdot H_R^2 - 1.213 \cdot H_R + 0.928 \quad (A17)$$

[Ding et al. \(2018, 2019\)](#).

Order of influence (based on  $\gamma$ -values): (A18)

Carbon steel: 1: temperature ( $T_w$ ); 2: dissolved oxygen ( $O_2$ ); 3: specific conductivity; 4: pH-value; 5: water pressure ( $p_w$ )

Copper: 1: temperature ( $T_w$ ); 2: salinity (Cl); 3: pH-value; 4: dissolved oxygen ( $O_2$ ); 5: fouling area (FA)

[Kovalenko et al. \(2017\)](#).

$$r_{corr} = \int_0^{\Delta t_E} r_{inc}[T_w(t_E), N_C(t_E), t_E] dt_E \quad (A19)$$

[Hicks and Oster \(2012\)](#).

$$r_{corr} = [0.0021 \cdot AK + (0.015 \cdot \log SRB + 0.0014 \cdot C_S)] - 0.0084 \quad (A20)$$

[Melchers and Ahammed \(2006\)](#).

$$c(t_E, E) = b(t_E, E) \cdot f_n(t_E, E) + \varepsilon(t_E, E) \quad (A21)$$

Here,  $c(t_E, E)$  is the weight loss (or pit depth),  $f_n(t_E, E)$  is a mean valued function,  $b(t_E, E)$  is a bias function,  $\varepsilon(t_E, E)$  is a zero mean error function,  $t_E$  is the exposure time, and  $E$  is a vector of environmental (and material) parameters.

## A3. Cathodic corrosion protection

[Diler et al. \(2019\)](#).

Effects of water temperature ( $T_w$ ) on protection current density.

Effects of water depth ( $D_w$ ) on protection current density.

[Bray \(1990\)](#) and [ISO/DIS 24656 \(2020\)](#).

Effects of water flow speed ( $v_F$ ) and dissolved oxygen ( $O_2$ ) concentration on protection current density.

[ISO/DIS 24656 \(2020\)](#).

$$FWZ = WL + H_{mo} \quad (A22)$$

Sea water velocity ( $v_F$ ) in 10 m depth increments.

[Okstad et al. \(2007\)](#).

Effects of water flow speed ( $v_F$ ) on the ratio Ca/Mg (calcareous deposits)

#### A4. Fouling

[Ameryoun et al. \(2019\)](#).

$$\Delta s = \frac{0.235}{1 + 6.94 \cdot \exp(-1.005 \cdot Ch)} \quad (A23)$$

[Page and Hubbard \(1987\)](#).

$$\Delta s = -0.11 \cdot \Delta s + 0.64 \cdot Ch + 9.67 \quad (A24)$$

[Page and Hubbard \(1987\)](#).

$$\Delta s = C \cdot 0.07 \cdot T_w \quad (A25)$$

## APPENDIX. BSENSOR REQUIREMENTS AND AVAILABILITY MATRICES

**Table B1**

Sensor requirements and availability matrix for atmospheric parameters identified in corrosion models and coating deterioration models

Situation	Reference	Meteorological parameter												
		T	RH	S <sub>d</sub>	P <sub>d</sub>	pH <sub>R</sub>	t <sub>R</sub>	T <sub>sun</sub>	R <sub>sun</sub>	UV	P	v <sub>w</sub>	WD	I
Atmosphere	ISO 9223 (2012)	M,F,R	M,F,R		C									M,R
	Bhaskar et al. (2004)	M,F,R	M,F,R		C									
	Feliu et al. (1993)	M,F,R	M,F,R		C		F,R							
	Vera et al., 2018	M,F,R	M,F,R		C								M,F,R	M,F,R
	Kihira et al. (2005)	M,F,R				C							M,F,R	
	Meira et al. (2008)					C	F,R						M,F,R	
	Corvo et al. (2008)						F,R						M,F,R	
	Santana et al. (2020)					C								
	Benarie and Lipfert (1986)													
	Chico et al. (2017)	M,F,R	M,F,R		C								M,F,R	
Coatings	Panchenko et al. (2012)	M,F,R											M,F,R	
	Gao et al. (2019)	M,F,R	M,F,R											
	Martin et al. (1994)	M,F,R											M,F	
	Mikhailov et al. (2001)	M,F,R	M,F,R										M,F,R	
	Tayler et al. (2015)	M,F,R	M,F,R										M,F	
	Momber et al. (2022)	M,F,R	M,F,R										M,F	

C - Copernicus, see Eq. (12); F - FINO initiative; M - MARNET network; R - RAVE initiative.

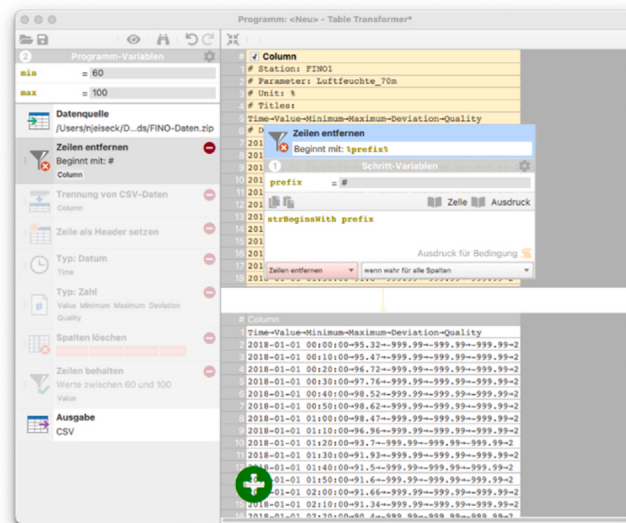
**Table B2**

Sensor requirements and availability matrix for oceanographic parameters identified in corrosion models

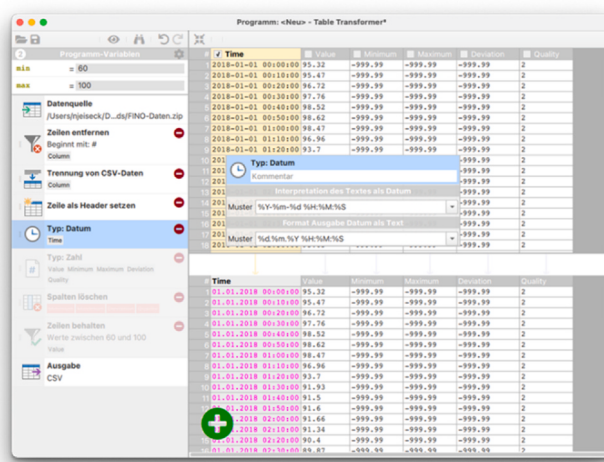
Situation	Reference	Oceanographic parameter												
		T <sub>w</sub>	v <sub>f</sub>	FD	O <sub>2</sub>	pH	Cl	H <sub>w</sub>	Ch	S <sub>c</sub>	P <sub>w</sub>	FA	D <sub>w</sub>	N <sub>c</sub>
Corrosion	Garbatov et al. (2011)	M,F,R	M,F,R	F,R				M						
	Guedes Soares et al. (2005)													
	Pedferri (2018)	M,F,R	M,F,R		M,R			M,F,R						
	Kovelenko et al. (2017)	M,F,R												
	Melchers and Ahammmmed (2006)	M,F,R	M,F,R			M,R								
	Khodabux et al. (2020)													R
	Hicks and Oster (2012)													
	Ding et al. (2018)	M,F,R			M,R	M						F	R	
	Ding et al. (2019)	M,F,R			M,R	M	M,F,R							
	Starokon (2020)	M,F,R	M,F,R					M,F,R						
Cathodic protection	Diler et al. (2019)	M,F,R												R
	Bray (1990)		M,F,R		M,R									
	ISO/DIS 24656 (2020)		M,F,R		M,R									
	Okstad et al. (2007)		M,F,R											
Fouling	Ameryoun et al. (2019)											M		
	Page and Hubbard (1987)	M,F,R										M		

M - MARNET network; F - FINO initiative; R - RAVE initiative.

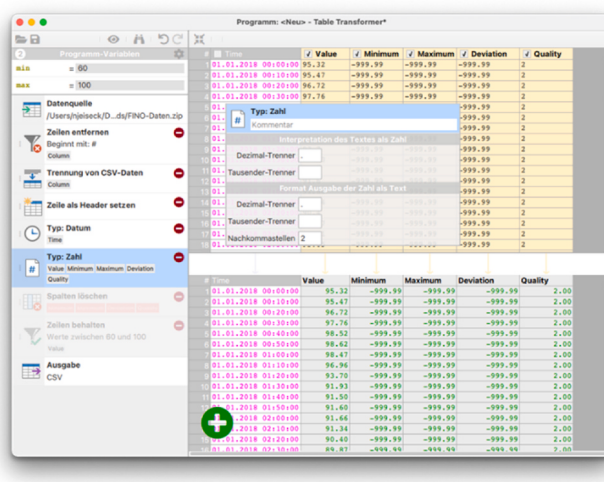
## APPENDIX C. SCREENSHOT USER INTERFACE TABLE TRANSFORMER: DATA INPUT, MANAGEMENT AND STORAGE



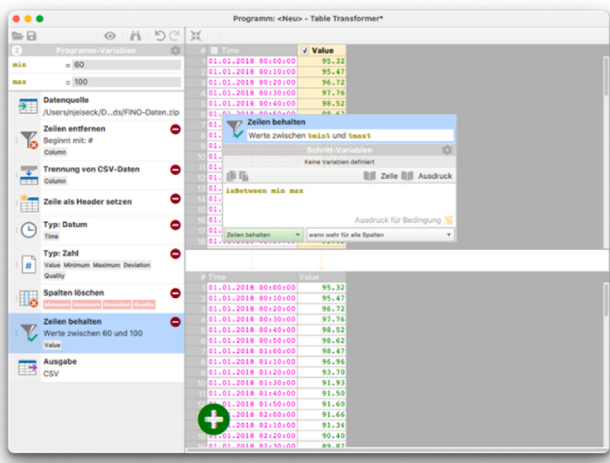
C1. Selection of input data



C2. Correction/formatting of time stamp



C3. Uniform data formatting



C4. Removal of defective/unsuitable data

## References

- Alcantara, J., Chico, B., Diaz, I., de la Fuente, D., Morcillo, M., 2015. Airborne chloride deposit and its effect on marine atmospheric corrosion of mild steel. Corrosion Sci. 97, 74–88. <https://doi.org/10.1016/j.corsci.2015.04.015>.
- Ameryoun, H., Schoefs, F., Barillé, L., Thomas, Y., 2019. Stochastic modeling of forces on jacket-type offshore structures colonized by marine growth. J. Mar. Sci. Eng. 7 (158), 1–28. <https://doi.org/10.3390/jmse7050158>.
- Baschek, B., Imai, J., 2011. Rogue wave observations off the US west coast. Oceanography 24, 158–165. <https://doi.org/10.5670/oceanog.2011.35>.
- Benarie, M., Lipfert, F.L., 1986. A general corrosion function in terms of atmospheric pollutant concentrations and rain pH. Atmos. Environ. 20 (10), 1947–1958. [https://doi.org/10.1016/0004-6981\(86\)90336-7](https://doi.org/10.1016/0004-6981(86)90336-7).
- Bhaskar, S., Iyer, N.R., Rajasankar, J., 2004. Cumulative damage function model for prediction of uniform corrosion rate of metals in atmospheric corrosive environment. Corrosion Eng. Sci. Technol. 39 (4), 313–320. <https://doi.org/10.1179/174327804X13172>.
- Bray, J.A., 1990. Design and Operational Guidance on Cathodic Protection of Offshore Structures, Subsea Installations and Pipelines. The Marine Technology Directorate Ltd., London, UK.
- BSH, 2020. RAVE Offshoreservice Projekt - Ozeanographische und strukturdynamische Messungen im Offshore Testfeld alpha ventus sowie die Weiterentwicklung von Monitoring-Konzepten für Offshore-Windparks. Abschlussbericht (01.02.2017 bis 31.01.2020). BSH, Hamburg, Germany. [https://www.bsh.de/DE/PUBLIKATIONEN/\\_Anlagen/Downloads-Projekte/RAVE/RAVE-quality-control-of-RAVE.pdf?\\_\\_blob=publicationFile&v=13](https://www.bsh.de/DE/PUBLIKATIONEN/_Anlagen/Downloads-Projekte/RAVE/RAVE-quality-control-of-RAVE.pdf?__blob=publicationFile&v=13).
- BSH, 2021. Real-time Data Quality Control in Situ Surface Waves (Version 1.3). BSH, Hamburg, Germany. [https://www.bsh.de/DE/DATEN/Klima-und-Meer/Seegang/\\_Anlagen/Downloads/manual\\_echtzeit-datenqualitaetskontrolle.pdf;jsessionid=FEFEDF7831B6C9D83C4D986F5ED7A31.live11311?\\_\\_blob=publicationFile&v=3](https://www.bsh.de/DE/DATEN/Klima-und-Meer/Seegang/_Anlagen/Downloads/manual_echtzeit-datenqualitaetskontrolle.pdf;jsessionid=FEFEDF7831B6C9D83C4D986F5ED7A31.live11311?__blob=publicationFile&v=3).
- Cai, Y., Zhao, Y., Ma, X., Zhou, K., 2020. Reliability assessment in dynamic field environment incorporating multiple environmental effects. Proc. Inst. Mech. Eng. O J. Risk Reliab. 234 (1), 3–14. <https://doi.org/10.1177/1748006X19879607>.
- Chico, B., de la Fuente, D., Diaz, I., Simancas, J., Morcillo, M., 2017. Annual atmospheric corrosion of carbon steel worldwide: an integration of ISOCORRAG, ICP/UNECE and MICAT databases. Materials 10 (601), 1–26. <https://doi.org/10.3390/ma10060601>.
- Christou, M., Evans, K., 2014. Field measurements of rogue water waves. J. Phys. Oceanogr. 44, 2317–2335. <https://doi.org/10.1175/JPO-D-13-0199.1>.
- Copernicus, 2020. COPERNICUS MARINE IN SITU TEAM, Copernicus In Situ TAC, Real Time Quality Control for Waves. CMEMS-INS-WAVES-RTQC.
- Corvo, F., Pérez, T., Martin, Y., Reyes, J., Dzib, L.R., Gonzalez, J.A., Castaneda, A., 2008. Corrosion research frontiers - atmospheric corrosion in tropical climate - on the concept of time of wetness and its interaction with contaminants deposition. In: Smithe, G.M. (Ed.), Electroanalytical Chemistry: New Research. Nova Science Publ., Inc., Hauppauge, NY, USA. Chapter 2.
- Diler, E., Larche, N., Thierry, D., 2019. Carbon Steel and Stainless-Steel Cathodic Protection Design Data in Deepsea Water - Influence of the Environment on the Biofilm Cathodic Activity. NACE Corrosion, 2019, Paper 13124, NACE Int., Houston, TX, USA, 2019.
- Ding, K., Guo, W., Qiu, R., Hou, J., Fan, L., Xu, L., . Corrosion behavior of Q235 steel exposed in deepwater of South China Sea. J. Mater. Eng. Perform. 27, 4489–4496. <https://doi.org/10.1007/s11665-018-3553-x>.
- Ding, K., Fan, L., Yu, M., Guo, W., Hou, J., Lin, C., 2019. Sea water corrosion behaviour of T2 and 12832 copper alloy materials in different sea areas. Corrosion Eng. Sci. Technol. 54 (6), 476–484. <https://doi.org/10.1080/1478422X.2019.1619289>.
- Errandonea, I., Beltran, S., Arrizabalaga, S., 2020. Digital Twin for maintenance: a literature review. Comput. Ind. 123, 103316. <https://doi.org/10.1016/j.compind.2020.103316>.
- Eurogoos, 2010. EUROGOOS DATA-MEQ WORKING GROUP, Recommendations for In-Situ Data Near Real Time Quality Control. Coriolis Data Centre.
- Feliu, S., Morcillo, M., Feliu Jr., S., 1993. The prediction of atmospheric corrosion from meteorological and pollution parameters - II. Long-term forecast. Corrosion Sci. 34 (3), 415–422. [https://doi.org/10.1016/0010-938X\(93\)90113-U](https://doi.org/10.1016/0010-938X(93)90113-U).
- Gao, J., Li, C., Lv, Z., Wang, R., Wu, D., Lia, X., 2019. The Establishment of Correlation Model between the Surface Aging of Organic Protective Coatings and Environmental Factors. Eurocorr 2019, Seville, Spain, 9–13 September, 2019.
- Garbatov, Y., Zayed, A., Guedes Soares, C., 2011. Corrosion modeling in marine structures, 2011. In: Guedes Soares, C., et al. (Eds.), Marine Technol. Engng. Taylor & Francis, London, pp. 1121–1156.
- Guedes Soares, C., Garbatov, Y., Zayed, A., Wang, G., 2005. Non-linear Corrosion Model for Immersed Steel Plates: Accounting for Environmental Factors. ABS Techn. Papers 2005, pp. 193–211.
- Hahn, J., Herklotz, K., Kreklau, M., Fischer, J.G., 2021. Ozeanographische Beobachtungen an Den FINO Stationen. Vortrag FINO-Konferenz, Kiel, Germany, 22.09.2021.
- Hicks, R.E., Oster, R.J., 2012. Developing a Risk Assessment Tool to Predict the Risk of Accelerated Corrosion to Port Infrastructure. Final Report to Grant DTMA1G10001, University of Minnesota Duluth, Department of Biology, Duluth, MN, USA, 3 March, 2012.
- Horstmann, T., Hinrichs, H., Kühne, U., 2015. Measurement System to Detect Salt Sediments (Corrosion) inside Offshore Wind Turbines. RAVE Offshore Wind R&D Conference 2015, Bremerhaven, Germany, pp. 13–15. October, 2015.
- IOOS, 2019. Manual for real-time quality control of in-situ surface wave data. In: QARTOD (Ed.), A Guide to Quality Control and Quality Assurance of In-Situ Surface Wave Observations. Version 2.1 ed.
- ISO 12944-2, 2018. Paints and Varnishes - Corrosion Protection of Steel Structures by Protective Paint Systems - Part 1: Classification of Environment. International Standard Organization, Geneva, Switzerland, 2018.
- ISO 9223, 2012. Corrosion of Metals and Alloys - Corrosivity of Atmospheres - Classification, Determination and Estimation. International Standard Organization, Geneva, Switzerland, 2012.
- ISO 9224, 2012. Corrosion of Metals and Alloys - Corrosivity of Atmospheres - Guiding Values for the Corrosivity Categories. International Standard Organization, Geneva, Switzerland, 2012.
- ISO/DIS 24656, 2020. Cathodic Protection of Offshore Wind Structures. International Standard Organization, Geneva, Switzerland, 2020.
- Khodabux, W., Causon, P., Brennan, F., 2020. Profiling corrosion rates for offshore wind turbines with depth in the North Sea. Energies 13, 2518. <https://doi.org/10.3390/en13102518>.
- Kihira, H., Senuma, T., Tanaka, M., Nishioka, K., Fujii, Y., Sakata, Y., 2005. A corrosion prediction method for weathering steels. Corrosion Sci. 47, 2377–2390. <https://doi.org/10.1016/j.corsci.2004.10.013>.
- Kovalenko, R., Melchers, R.E., Chernov, B., 2017. Long-term immersion corrosion of steel subject to large annual variations in seawater temperature and nutrient concentration. Struct. Infrastruct. Engng. 13 (8), 978–987. <https://doi.org/10.1080/15732479.2016.1229797>.
- Leiding, T., Tinz, B., Gates, L., Rosenhagen, G., Herklotz, K., Senet, C., 2016. Standardisierung und vergleichende Analyse der meteorologischen FINO-Messdaten (FINO 123). Forschungsvorhaben FINO-Wind (Abschlussbericht: 12/2012-04/2016), Hamburg, Germany.

- Martin, J.W., Saunders, S.C., Floyd, F.L., Wineburg, J.P., 1994. Methodologies for Predicting the Service Lives of Coating Systems. NIST Building Science Series No. 172, Gaithersburg, MD, USA: Nat. Inst. Standards Technol., October 1994.
- Meira, G.R., Andrade, C., Alonso, C., Padaratz, I.J., Borba, J.C., 2008. Modelling sea-salt transport and deposition in marine atmosphere zone - a tool for corrosion studies. Corrosion Sci. 50, 2724–2731. <https://doi.org/10.1016/j.corsci.2008.06.028>.
- Melchers, R.E., 2012. Modeling and prediction of long-term corrosion of steel in marine environments. Int. J. Offshore Polar Eng. 22 (4), 257–263.
- Melchers, R.E., Ahammed, M., 2006. Statistical characterization of corroded steel plate surfaces. Adv. Struct. Eng. 9 (1), 83–90. <https://doi.org/10.1260/136943306776232828>.
- Mikhailov, A.A., 2001. Dose-response functions as estimates of the effect of acid precipitates on materials. Protect. Met. 37 (4), 357–366. <https://doi.org/10.1023/A:1010447510562>.
- Momber, A.W., 2022. Corrosion and Corrosion Protection of Wind Power Structures in Marine Environments, Vol. 1: Introduction and Corrosive Loads. Elsevier, London.
- Momber, A.W., Nattkemper, T.W., Langenkämper, D., Möller, T., Brün, D., Schaumann, P., Shojai, S., 2021a. Digitalisierung und die Verarbeitung von Sensordaten für die Zustandsbewertung von Oberflächenschutzsystemen von stählernen Türmen von Onshore-Windenergieanlagen. Stahlbau 90 (7), 528–541. <https://doi.org/10.1002/stab.202100020>.
- Momber, A.W., Möller, T., Langenkämper, D., Nattkemper, T.W., Brün, D., 2021b. A Digital Twin concept for the prescriptive maintenance of protective coating systems on wind turbine structures. Wind Eng. <https://doi.org/10.1177/0309524X211060550>.
- Momber, A.W., Nattkemper, T.W., Langenkämper, D., Möller, T., Brün, D., Schaumann, P., Shojai, S., 2022. A data-based model for condition monitoring and maintenance planning for protective coating systems for wind tower structures. Renew. Energy 186, 957–973. <https://doi.org/10.1016/j.renene.2022.01.022>.
- Müller, M., 2008. Sauerstoffdynamik der Nordsee - Untersuchungen mit einem dreidimensionalen Ökosystemmodell. Dissertation, Universität Hamburg, Hamburg, Germany, 2008.
- Okstad, T., Rannestad, O., Johnsen, R., Nisancioglu, K., 2007. Significance of hydrogen evolution during cathodic protection of carbon steel in seawater. Corrosion 63 (9), 857–865. <https://doi.org/10.5006/1.3278436>.
- Page, H.M., Hubbard, D.M., 1987. Temporal and spatial patterns of growth in mussels *Mytilus edulis* on an offshore platform: relationships to water temperature and food availability. J. Exp. Mar. Bioi. Ecol. 111, 159–179. [https://doi.org/10.1016/0022-0981\(87\)90053-0](https://doi.org/10.1016/0022-0981(87)90053-0).
- Panchenko, Y.M., Strelakov, P.V., Zhilikov, V.P., Karimova, S.A., Berezina, L.G., 2012. Corrosion resistance of D16 alloy depending on the salinity and meteorological parameters of coastal atmosphere. Protect. Met. Phys. Chem. Surface 48 (7), 740–750. <https://doi.org/10.1134/S2070205112070118>.
- Pedderferri, P., 2018. Corrosion Science and Engineering. Springer, Cham, Switzerland.
- Santana, J.J., Cano, V., Vasconcelos, H.C., Souto, R.M., 2020. The influence of test-panel orientation and exposure angle on the corrosion rate of carbon steel: mathematical modeling. Metals 10 (196), 1–13. <https://doi.org/10.3390/met10020196>.
- SEADATANET, 2010. Data Quality Control Procedures. Version 2.0 ed.
- Shinohara, T., Motoda, S., Oshikawa, W., 2005. Evaluation of corrosivity in atmospheric environment by ACM (Atmospheric Corrosion Monitor) type corrosion sensor. Mater. Sci. Forum 475–479, 61–64. <https://doi.org/10.4028/www.scientific.net/MSF.475-479.61>.
- Starokon, I.V., 2020. Rating of corrosion factors determining its speed for stationary offshore platforms for oil, gas, coal and other minerals. J. Phys.: Conf. Ser. 1515, 032032 <https://doi.org/10.1088/1742-6596/1515/3/032032>.
- Tayler, M.L., Blanton, M., Konecki, C., Rawlins, J., Scully, J.R., 2015. Scribe creep and underpaint corrosion on ultra high molecular weight epoxy resin coated 1018 steel (UNSG10180), Part II: scribe creep model as a function of environmental severity factors. Corrosion 71 (3), 326–342. <https://doi.org/10.5006/1349>.
- Tchakoua, P., Wamkeue, R., Ouhrouche, M., Slaoui-Hasnaoui, F., Tameghe, T.A., Ekem, G., 2014. Wind turbine condition monitoring: state-of-the-art review, new trends, and future challenges. Energies 7, 2595–2630. <https://doi.org/10.3390/en7042595>.
- Tidblad, J., Mikhailov, A.A., Kucera, V., 2000. Model for the prediction of the time of wetness from average annual data on relative air humidity and air temperature. Protect. Met. 36 (6), 533–540. <https://doi.org/10.1023/A:1026621009635>.
- Vera, R., de Rincon, O., Bagnara, M., Romero, N., Araya, R., Ossandon, S., 2018. Tropical/non-tropical marine environments impact on the behaviour of carbon steel and galvanised steel. Mater. Corros. 65 (5), 614–625. <https://doi.org/10.1002/maco.201709873>.
- Weiss, M., 2011. Analyse der Nutzungsmöglichkeiten von biologischem Aufwuchs von künstlichen Hartsubstraten für die Gewinnung alternativer Protein- und Lipiddressurcen. Endbericht des Projektes „NutriMat“, Inst. für Marine Ressourcen GmbH, Bremerhaven, Germany.
- Zhang, H., Yan, J., Han, S., Li, L., Liu, Y., Infield, D., 2021. Uncertain accessibility estimation method for offshore wind farm based on multi-step probabilistic wave forecasting. IET Renew. Power Gener. 15 (3), 2944–2955. <https://doi.org/10.1049/rpg2.12227>.
- A<sub>1–7</sub>:** constants  
**AK:** alkalinity  
**B:** corrosion function power exponent  
**BSh:** Federal Maritime and Hydrographic Agency  
**C:** constant  
**C<sub>corr</sub>:** corrosion attribute  
**C<sub>h</sub>:** chlorophyll-a concentration  
**c<sub>s</sub>:** sensitivity factor  
**C<sub>l</sub>:** seawater chloride concentration  
**C<sub>S</sub>:** sulphate content  
**D:** rating parameter  
**D<sub>H</sub>:** water depth  
**D<sub>L</sub>:** local deterioration degree  
**D<sub>w</sub>:** water depth  
**E:** activation energy  
**FA:** fouling area  
**f<sub>NN</sub>:** artificial neural network model-based factor  
**f<sub>t</sub>:** air temperature function  
**FWL:** frequently wetted zone  
**FD:** water flow direction  
**g(D):** limit-state function  
**H:** atmospheric height  
**h<sub>C</sub>:** corrosion depth  
**H<sub>mo</sub>:** significant wave height  
**H<sub>R</sub>:** relative water depth  
**H<sub>W</sub>:** mean monthly wave height  
**I:** surface inclination  
**k:** shape parameter  
**k<sub>r</sub>:** constant  
**MAQ:** marine atmosphere quality parameter  
**MARNET:** Marine environment monitoring network  
**N<sub>C</sub>:** nutrient concentration  
**N<sub>d</sub>:** number of rainy days  
**O:** surface orientation  
**O<sub>2</sub>:** dissolved oxygen concentration  
**O<sub>2B</sub>:** oxygen concentration in bulk seawater  
**P:** precipitation  
**p<sub>A</sub>:** air pressure  
**P<sub>d</sub>:** average annual SO<sub>2</sub> deposition rate  
**p<sub>w</sub>:** water pressure  
**pH:** seawater pH-value  
**pH<sub>R</sub>:** rain pH-value  
**R:** resistance effect  
**r<sub>cor</sub>:** corrosion rate  
**Rf:** rainfall intensity  
**R<sub>G</sub>:** gas constant  
**RH:** average annual relative air humidity  
**r<sub>i</sub>:** factor corrosion rate  
**r<sub>inc</sub>:** incremental corrosion rate  
**R<sub>sun</sub>:** total solar radiation  
**S:** load effect  
**S<sub>C</sub>:** specific conductivity  
**S<sub>d</sub>:** average annual chloride deposition rate  
**S<sub>do</sub>:** average annual chloride deposition rate at the shore  
**SRB:** sulphate-reducing bacteria  
**T:** average annual air temperature  
**t<sub>E</sub>:** exposure time  
**TOW:** time of wetness  
**T<sub>W</sub>:** seawater temperature  
**UV:** ultraviolet radiation  
**v<sub>dep</sub>:** deposition velocity  
**v<sub>F</sub>:** seawater flow velocity  
**v<sub>W</sub>:** wind velocity  
**WD:** wind direction  
**WL:** water level  
**X:** distance from shoreline  
**X<sub>p</sub>:** material parameter  
**Y<sub>f</sub>:** external (environmental) parameter  
**Z:** index of regional corrosivity  
**a:** constant  
**a<sub>1</sub>:** constant  
**δ:** constant  
**Δs:** shell length  
**Δs<sub>i</sub>:** shell growth rate  
**Δt:** time increment  
**ε:** constant  
**κ:** constant  
**λ:** scale parameter

## Glossary

A: first-year corrosion rate